This is a preprint, the final version is subject to change, of the American Mineralogist (MSA)
Cite as Authors (Year) Title. American Mineralogist, in press.
(DOI will not work until issue is live.) DOI: http://dx.doi.org/10.2138/am-2016-5422

Revision 1:

A single-crystal X-ray and Raman spectroscopic study of hydrothermally synthesized arsenates and vanadates with the descloizite and adelite structure types

TAMARA ĐORĐEVIĆ,[1] UWE KOLITSCH,[2,1] AND LUTZ NASADALA[1]

[1]Institut für Mineralogie und Kristallographie, Geozentrum, Universität Wien, Althanstraße 14, 1090 Wien, Austria

[2]Mineralogisch-Petrographische Abt., Naturhistorisches Museum, Burgring 7, A-1010 Wien, Austria

ABSTRACT

Studying the reason for the formation of two structural sub-types, seven arsenate and vanadate compounds of descloizite and adelite groups, $CdCo(OH)(AsO_4)$ (**1**), $CdCu(OH)(AsO_4)$ (**2**), $SrCo(OH)(AsO_4)$ (**3**), $SrZn(OH)(AsO_4)$ (**4**), $SrCu(OH)(VO_4)$ (**5**), $CdCo(OH)(VO_4)$ (**6**), and $CdCu(OH)(VO_4)$ (**7**) were synthesized under low-temperature hydrothermal conditions. **1**-**2** and **6**-**7** are isostructural with descloizite- and **3**-**5** with adelite- group minerals and several synthetic compounds. Together with a sample of conichalcite, $CaCu(OH)(AsO_4)$ (**8**), they were investigated using single-crystal X-ray diffraction [$R(F)$ = 0.0153–0.0283 for **1**–**5** and **8;** for **6** and **7,** $R(F)$ = 0.0603 and 0.0444, respectively] and Raman spectroscopy. Although crystallizing in different orthorhombic space groups, the atomic arrangements of descloizite-

(*Pnam*) and adelite- ($P2_12_12_1$) type compounds adopt the same topology: the atomic arrangement is characterized by $M2O_6$ octahedrons ($M2$ = Mg^{2+}, Al^{3+}, $Mn^{2+,3+}$, Fe^{2+}, Co^{2+}, Ni^{2+}, Cu^{2+}, Zn^{2+}) edge-linked into chains. These chains are interconnected by XO_4 tetrahedrons (X = Si^{4+}, P^{5+}, V^{5+}, As^{5+}, Mo^{6+}) into a three-dimensional framework. Cavities host $M1$ atoms ($M1$ = Na^{+}, Ca^{2+}, Cd^{2+}, Hg^{2+}, Pb^{2+}); their coordination varies from [7] for descloizite-type representatives to [8] for adelite-type structures. The OH stretching frequencies in the Raman spectra are in good agreement with the observed O–H···O donor-acceptor distances. A detailed discussion of the crystal chemistry of these compounds and its influence on the space-group symmetry indicate a distinct dependence of the structural changes on the average ionic radii $(r_{M1} + r_X)/2$.

INTRODUCTION

The descloizite supergroup of minerals currently comprise 17 members (Table 1 and references therein). The large majority of the members are arsenates and vanadates occurring in a considerable variety of ore deposits and on mine dumps. They were formed either by weathering of the primary ores or by hydrothermal processes. Up to now, there were just a few reports on hydrothermally synthesized synthetic members of these compounds (Clearfield et al. 1977, Moini et al. 1986, Permer et al. 1993, Healey et al. 1999, Effenberger 2002, Weil 2004).

The general formula of descloizite supergroup of minerals and compounds is $M1^{1+,2+}M2^{2+,3+}(OH,O)[X^{4+,5+,6+}(O_4,O_3OH)]$ ($M1$ = Na^{+}, Ca^{2+}, Cd^{2+}, Hg^{2+}, Pb^{2+}; $M2$ = Mg^{2+}, Al^{3+}, $Mn^{2+,3+}$, Fe^{2+}, Co^{2+}, Ni^{2+}, Cu^{2+}, Zn^{2+}; X = Si^{4+}, P^{5+}, V^{5+}, As^{5+}, Mo^{6+}). Representatives with $M1$ = Na^{+}, Cd^{2+}, and Hg^{2+}, and X = Mo^{6+} were found only for synthetic members. All members are orthorhombic (Z = 4), with a common topology. The atomic arrangement is

characterized by $M2O_6$ octahedrons (elongated tetragonal bipyramids in case of Cu^{2+} or Mn^{3+} cations due to Jahn-Teller distortion) edge-linked into chains. These chains are interconnected by XO_4 tetrahedrons into a three-dimensional framework. Cavities host *M*1 atoms; their coordination varies from [7] to [8] depending on the space-group symmetry. The atomic arrangement exhibits two distinct structural varieties. They are distinguished by their space-group symmetries and the coordination numbers [7] and [8] for the *M*1 cations, respectively. These varieties are responsible for classifying the compounds into two subdevisions. The parental structure is centrosymmetric and shows space-group symmetry *Pnam* [descloizite-type compounds with *M*1 = Cd^{2+}, Hg^{2+}, Pb^{2+}, *M*2 = Mn^{2+}, Fe^{2+}, Cu^{2+}, Zn^{2+}, and *X* = V^{5+}, Mo^{6+}]. This symmetry was proved for four minerals, all of which are vanadates with *M*1 = Pb^{2+}, and four synthetic compounds (Table 1). The adelite-type compounds show a slight deviation from centrosymmetry, and crystallize in space group $P2_12_12_1$. Representatives are known for *M*1 = Ca^{2+} or Pb^{2+}, *M*2 = Mg^{2+}, Al^{3+}, Mn^{3+}, Fe^{2+}, Ni^{2+}, Co^{2+}, Cu^{2+}, Zn^{2+}, and *X* = Si^{4+}, P^{5+}, As^{5+}, V^{5+}. Thus, the variability of chemical composition in this group is quite large: arsenates, vanadates, protonated silicates, molybdates, and phosphates (Schlüter et al. 2011). Compounds adopting this space group are also of general interest because they are acentric. For the mineral gabrielsonite, $PbFe^{2+}(OH)(VO_4)$, the structural data are uncertain. The space group of gabrielsonite, originally reported as $P2_1ma$ (Moore 1967), is unconfirmed; a single-crystal study by the second author of this paper suggested other possible space groups, but was unable to solve the structure in either orthorhombic or lower-symmetry space groups (features observed during trials solutions strongly indicated the presence of microtwinning). An intermediate (Pb,Ca) solid-solution member, "β-duftite", $(Pb,Ca)Cu(OH)(AsO_4)$ (Guillemin 1956), which appears to be a simple chemical intermediate between duftite and conichalcite, was shown to have an incommensurately modulated superstructure (Kharisun et al. 1998). Although crystallizing in space group $P2_12_12_1$ and having similar unit-cell parameters as the members of the adelite group, $NaZnSiO_3OH$ (Table 1), has tetrahedrally

coordinated Zn (*M*2) atoms. Its structure consists of an array of ZnO_4 and SiO_3OH tetrahedrons, which form eight-membered rings along the crystallographic *c* direction. The Na^+ ions are situated in these channels with five close contacts and one longer contact to the framework oxygens. The authors describing $NaZnSiO_3OH$ (Healey et al. 1999) have not discussed any connection to the adelite-group compounds.

The knowledge on synthetic members of these compounds was poor prior to the present study (Table 1). Only one of five reported synthetic compounds is acentric ($NaZnSiO_3OH$) and for the other four, centrosymmetry was proven. Among the minerals, only conichalcite and duftite (Guillemin 1956), vuagnatite (Leistner and Chatterjee, 1978) and impure mottramite, $(Pb_{0.7}Fe_{0.3})Cu(VO_4)(OH)_{0.5}O_{0.4}$ (Permer et al. 1993), were synthesized; for a critical comments on the reported formula of the latter, see the footnote in Table 1.

An ongoing study on the hydrothermal synthesis, crystallography, and properties of arsenate(V) and vanadate(V) compounds in the *M*1O–*M*2O–X_2O_5–H_2O system (*M*1 = Sr^{2+}, Cd^{2+}, Ba^{2+}, Bi^{3+}, Hg^{2+}; *M*2 = Mg^{2+}, $Mn^{2+,3+}$, $Fe^{2+,3+}$, Co^{2+}, Ni^{2+}, Cu^{2+}, Zn^{2+}; X = V^{5+}, As^{5+}) yielded a large number of new *M*1^{2+}–(H–)-, *M*2^{2+}–(H–)- and *M*1–*M*2–(H–) arsenates and vanadates (Mihajlović and Effenberger 2004, 2006, Mihajlović et al. 2004a,b, Đorđević 2008a,b, 2010, Đorđević et al. 2008, Weil et al. 2009, Đorđević and Karanović 2008, 2010, Đorđević 2011, Stojanović et al. 2012, Đorđević and Karanović 2013, Đorđević and Kolitsch 2013, Đorđević et al. 2015, Kovač et al. 2015) that were characterized structurally, and, in part, also by spectroscopic techniques. Among them, seven new synthetic members with adelite- and descloizite-type crystal structures, $CdCo(OH)(AsO_4)$ (**1**), $CdCu(OH)(AsO_4)$ (**2**), $SrCo(OH)(AsO_4)$ (**3**), $SrZn(OH)(AsO_4)$ (**4**), $SrCu(OH)(VO_4)$ (**5**), $CdCo(OH)(VO_4)$ (**6**), and $CdCu(OH)(VO_4)$ (**7**) were synthesised, which are the subject of the present study. A preliminary report on **1**-**3** and **5**-**6** was given by Đorđević (2007). Note that compound **2** was also briefly reported, with atom coordinates, in an one-page conference abstract (Effenberger

2002); these coordinates are not included in the latest edition of the ICSD database. Furthermore, a sample of well-crystallized conichalcite (**8**) from the Maria Catalina mine, Pampa Larga district, Copiapó Province, Chile, was also re-investigated.

In addition to presenting new results on the hydrothermal synthesis, crystal structures and spectroscopic data of the novel seven adelite- and descloizite-type arsenates and vanadates, we provide herein some discussion of the structural distortion and the measure of similarity among these compounds, as well as a brief discussion on the structural relations to chemically and topologically similar mineral groups. The names of the groups and the terminology used for the classification (group hierarchy) are not the one recognized by IMA CNMNC (Mill et al. 2009).

EXPERIMENTAL

Materials

For the low-temperature hydrothermal synthesis of compounds **1-7**, the following reagents were used in stoichiometric quantities: $Cd(OH)_2$ (Alfa Products 89297), $3As_2O_5{\cdot}5H_2O$ (Merck, 99 %) and Cu and Co powders (manufacturer unknown), for **1** and **2**, respectively, $Sr(OH)_2{\cdot}8H_2O$ (Merck 7876, > 97%), $Co(OH)_2$ (Alfa Products 89178), As_2O_5 (Alfa Products 87687, > 99.9 %) for **3**, $Sr(OH)_2{\cdot}8H_2O$ (Sigma-Aldrich, 415-219-500G), ZnO (Sigma-Aldrich, 255750-100g), As_2O_5 (Alfa Products 87687, > 99.9 %) and ionic liquid, 1-ethyl-3-methyl-imidazolium bromide (Fluka 03938-25G) for **4**, $Sr(OH)_2{\cdot}8H_2O$ (Merck 7876, > 97%), Cu powder (manufacturer unknown) and As_2O_5 (Alfa Products 87687, > 99.9 %) for **5**, and Cd(OH)2, As_2O_5 (Alfa Products 87687, > 99.9 %), Co and Cu powders for **6** and **7**, respectively.

The mixtures were transferred into Teflon vessels and filled to approximately 80 % of their inner volume with distilled water. Subsequently, they were enclosed into stainless steel

autoclaves and heated under autogeneous pressure under the following heating and cooling conditions: for compounds **1** and **2**, starting mixtures were heated from room temperature to 220 °C, held at that temperature for 96 h, and then furnace-cooled to room temperature. The mixture for **3** was heated from 20 to 220 °C (4 h), held at that temperature (48 h), cooled to 150 °C (10 h), kept at this temperature (10 h), cooled to 100 °C (10 h), kept at this temperature (10 h), and finally cooled to room temperature (10 h). The mixtures for **4**-**7** were heated from 20 to 220 °C (4 h), held at that temperature (72 h), and cooled to room temperature (72 h). Compound **1** crystallized as pink, prismatic crystals up to 0.16 mm in length (yield 40%), together with colourless, transparent, prismatic crystals of $Cd_5(AsO_4)_3Cl_{0.58}(OH)_{0.42}$ (Đordević et al. 2008) (yield 35%) and $Co_{1-x}(OH)_3(AsO_4H_{2x/3})(HAsO_4)$ (Huges et al. 2003) (yield 25%). Compound **2** crystallized as green, prismatic crystals up to 0.2 mm in length (yield 60%) together with blue crystals of $Cu_3(AsO_4)_2$-III (Effenberger 1988) (yield 40 %). Compound **3** was obtained as light pink, prismatic crystals up to 0.15 mm in length (yield 50 %), together with a volumetrically similar amount of colourless, prismatic crystals of $Sr_5(AsO_4)_3F$ (Đordević et al. 2008). Compound **4** formed colorless prismatic crystals up to 0.20 mm in length (yield 55 %) together with prismatic crystals of $Zn_2(AsO_4)(OH)$ (Hill 1976) (yield 45%). Compound **5** crystallized as green, transparent, acicular crystals up to 0.1 mm in length (yield 25 %), accompanied by large, green prisms of a new cadmium-vanadate $Cd_5(VO_4)_2(OH)_4$ (to be published elsewhere) and undissolved parts of the starting mixture. Very subordinate (yield 5 %) dark pinkish-brown prismatic crystals were obtained for compound **6**. Dark olive green, prismatic crystals of **7** crystallized together with dark-green, prismatic crystals of $Cd_2V_2O_7$ (Sokolova et al. 1986) (yield 40 %), and undissolved parts of the starting mixture. We point out that attempts to synthesize any Ba analogues were all unsuccessful, indicating that the Ba^{2+} cation is too large for both descloizite and adelite structure types.

A mineral sample of conichalcite (**8**) showing bright green, chisel-shaped prisms from the Maria Catalina mine, Pampa Larga district, Copiapó Province, Chile, associated with pale bluish, indistinct crystals of rruffite ($Ca_2Cu(AsO_4)_2{\cdot}2H_2O$, Yang et al. 2011), mansfieldite, and baryte, was also re-investigated. A preliminary report on the results was given in a conference abstract (Đorđević and Kolitsch, 2008).

X-ray diffraction experiments and crystal-structure determinations

Room-temperature intensity data of all crystals were collected on a Nonius KappaCCD single-crystal four-circle diffractometer (Mo$K\alpha$-radiation, graphite monochromator), equipped with a 300 mm diameter capillary-optics collimator. Unit-cell parameters were determined with HKL SCALEPACK (Nonius, 2005-2007). A complete sphere of reciprocal space (φ and ω scans) was measured up to 30-35° 2θ for **1** and **3**-**7**. Samples **2** and **8** were measured assuming orthorhombic symmetry. The intensity data were processed with the Nonius program suite DENZO-SMN (Nonius, 2005-2007) and corrected for absorption by the multi-scan method (Otwinowski et al. 2003). All structures were solved by direct methods using SIR97 (Altomare et al. 1999) and refined on F^2 by full-matrix least-squares using SHELXL97 (Sheldrick 2008) implemented in WinGX (Farrugia 2012). Anisotropic displacement parameters were allowed to vary for all atoms; only for the H atoms, located from difference-Fourier maps, isotropic displacement parameters were refined. For **1**-**5** the positions of hydrogen atoms were refined with a restrained O–H distance of 0.89(2) Å. The U_{iso} values of the H atoms were refined freely. Note that, considering the unusually high, most positive peaks (next to the *M*1 site) in the difference-Fourier maps for both **1** (Cd-Co-As-member, with 2.04 e^- at a distance of 0.79 Å from Cd, the next-highest peak being 0.96 e^- at a distance of 1.44 Å from O1) and **4** (Sr-Zn-As member, with 2.5 e^- at a distance of 0.76 Å from Sr, the next-highest peak being 1.02 e^- at a distance of 0.74 Å from O5) and, additionally, the distinctly anisotropic displacement ellipsoid for Cd in **1**, an anisotropic split-

172 *M*1 model was also tried for both **1** and **4**. For **1** this model led to the disappearance of this
173 high peak (now the highest peak was 0.93 e^-, at a distance of 1.45 Å from O1) and reduced *R*1
174 from 2.81% to 1.99%. The refined occupancy ratio for the two split positions [CdA:
175 0.0149(5), 0.0062(4), 0.0280(17), CdB: 0.0152(15), 0.0045(12), 0.112(10)] was
176 0.72(8):0.28(8); the CdA-CdB distance was 0.11(8) Å, the CdB position was still fairly
177 anisotropic while the CdA position was only very slightly anisotropic. With respect to the
178 latter observation, it is worthy noting that the model did not work if the two split positions
179 were constrained to have identical U_{anis} values. Since the split-*M*1 model indicates only
180 negligible positional splitting of the *M*1 site in **1**, but distinct volumetric splitting (with,
181 however, the caveat of still distinctly anisotropic behavior of CdB), a splitting seems possible,
182 but not fully provable, also considering possible artefacts of the absorption correction. Thus,
183 we have preferred to retain the unsplit model. For **4** the split-*M*1 model led also to the
184 disappearance of this high peak (now the highest peak was 1.14 e^-, at a distance of 1.1 Å from
185 As) and reduced *R*1 from 2.83% to 2.46%. The refined occupancy ratio for the two split
186 positions [SrA: 0.63581(4), 0.33111(4), 0.47585(7), SrB: 0.6471(15), 0.3140(12), 0.592(3),
187 with a constraint to have identical U_{anis} values] was 0.9706(12):0.0294(12); the SrA-SrB
188 distance was 0.721(16) Å. Since the split-*M*1 model indicates only negligible volumetric
189 splitting in **4**, the unsplit model was preferred, also to facilitate comparisons with the other
190 members. Selected crystal and experimental data are given in Table 2. The final atomic
191 coordinates and anisotropic displacement parameters are given in Tables 3 and 4,
192 respectively. Selected bond distances and bond angles are listed in Table 5 and the results of
193 bond-valence calculations are given in Table 6. All drawings of crystal structures were
194 produced with ATOMS (Dowty 2000).

195 The single-crystal studies of $CdCo(OH)(VO_4)$ (**6**) and $CdCu(OH)(VO_4)$ (**7**) suggested
196 space group *Pnam* (based on extinction conditions and intensity statistics), but the refinements
197 revealed unexplained anomalies in the obtained models, despite reasonably low *R*(*F*) values

of 0.058 for **6** and 0.045 for **7**. Distinctly anisotropic displacement ellipsoids were observed for the O1 and, more pronouncedly, O2 sites in **6**. The O1 (OH) site is bonded to Cd, Co, and V, while the O2 site is bonded to Cd and V only. In contrast, for **7** similarly anomalous displacement ellipsoids were shown by the O3 site and, less so, by the O4 and O2 sites. A splitting of the O3 site, suggested by the refinement software, resulted in physically impossible displacement parameters for one of the two subsites. A trial refinement of **6** in $P2_12_12_1$, assuming racemic twinning, gave $R(F) = 0.058$ and a Flack parameter of 0.7(2), suggesting that the centrosymmetric model was more plausible; again three O sites (O2-4) showed more or less anomalous displacement ellipsoids. In order to verify the possible presence of any supercells in **6** or **7**, both measured crystals were also studied with a Stoe StadiVari single-crystal diffractometer equipped with a Incoatec μ-source and a high-sensitivity Dectris Pilatus 300K hybrid-pixel detector. The recorded images showed a complex combination of twinning features and modulation. No structure refinement was attempted. The reason for the anomalous features and the modulation in **6** and **7** might be the fact that the Cd^{2+} cation in the two compounds is smaller than all the other divalent cations that form descloizite-type structures (Ca^{2+}, Sr^{2+}, Pb^{2+}). In combination with a large *X* cation (V^{5+}), this might result in an incipient instability of the *Pnam* atomic arrangement, possibly compensated for by the observed modulation. We point out that no anomalies were observed for the two Cd members containing the smaller As^{5+} cation, $CdCo(OH)(AsO_4)$ (**1**) and $CdCu(OH)(AsO_4)$ (**2**). The average structure models in *Pnam* for **6** and **7** are given in Supplemental materials, Tables S1 and S2.

Chemical composition

The chemical composition of the conichalcite sample from the Maria Catalina mine was established by means of quantitative electron probe microanalyser (EPMA) measurements,

which were performed on a Cameca SX100 instrument at an accelerating voltage of 15 kV and a beam current of 20 nA; the counting time was 20 s for each element. The EPMA data revealed a near-end member composition, however with significant zoning of very minor impurity elements (Na, Sr, Zn, Mg, Al, P, S, and Si). Most zones are less than 1 μm thick (Fig. 1), and the precise chemical composition of each zone was not measurable. Electron microprobe analysis yielded (wt.%): CaO 20.02, SrO 0.14, Na_2O 0.11, CuO 28.32, ZnO 0.52, Al_2O_3 0.22, MgO 0.04, As_2O_5 42.65, P_2O_5 0.35, SO_3 0.14, SiO_2 0.02, sum 92.54. The idealized empirical formula derived from the EPMA results is $Ca(Cu_{0.97}Zn_{0.02}Mg_{0.01})(OH)[(As_{0.97}P_{0.03})O_4]$. The crystal-structure refinement of a visually identical crystal from the same specimen yielded the somewhat Mg-richer formula $Ca(Cu_{0.92}Mg_{0.08})(OH)(AsO_4)$. Both formulae are slightly different from the previously reported formula $Ca(Cu_{0.99}Zn_{0.01})(OH)(AsO_4)$ of a conichalcite sample from the same Chilean locality (Henderson et al. 2008), and from the formulae of structurally studied samples from the Gozaisho mine, Japan [$Ca(Cu_{0.87}Mg_{0.13})(AsO_4)(OH)$] and the Higgins mine, Arizona, USA [$Ca(Cu_{0.96}Mg_{0.04})(AsO_4)(OH)$] (Sakai et al., 2009). We point out that the presence of racemic twinning in the sample of Henderson et al. (2008) is unclear. These authors described their sample as "naturally twinned", and in their supplementary material it is stated "it turned out that the measured crystal was racemically twinned with an approximate twin fraction of 4:1 (BASF = 0.21)". In apparent contrast to the latter, the Flack parameter was quoted as "0.00(2)" (Table and cif-file presented by Henderson et al., 2008). Sakai et al. (2009) did not state whether their samples were racemically twinned or not. The Flack parameter in our refinement was determined at 0.037(15).

Raman spectroscopy

To obtain further information on the anion groups and especially on hydrogen bonds, Raman spectra were acquired. Unpolarised Raman spectra of **3** and **8** were obtained with a Renishaw RM1000 spectrometer equipped with Leica DMLM optical microscope, an optical grating with 1200 grooves/mm, and Si-based charge-coupled device (CCD) detector. Spectra were excited with the He–Ne 632.8 nm line (8 mW). The beam was focused to the sample surface using a Leice 50× objective (N.A. = 0.75). Raman spectra of **1**, **2**, **4**, and **5** were measured with a Horiba LabRam–HR system equipped with Olympus BX41 optical microscope, a 1800 grooves/mm grating in the beam path, and Si-CCD. Spectra were obtained with the 632.8 nm emission of a He–Ne laser (10 mW) or the 473 nm emission of a diode laser (3 mW). An Olympus 100× objective (N.A. = 0.90) was used. In all cases the density of the laser power was well below the threshold for possible sample changes due to intense laser-light absorption and resulting temperature increase. The spectral resolution was between ~3 cm–1 (RM1000 system) and ~0.8 cm–1 (Evolution system, red spectral range), and the lateral resolution was about 3µm (RM1000) and 1.5 µm (Evolution), respectively.

RESULTS AND DISCUSSION

Description of the crystal structures

In the synthesized adelite-type representatives (**3-5**), all atoms lie on a general position and have site symmetry 1. It is worthy of note that among these compounds only **4** was racemically twinned [refined twin ratio 0.446(19):0.554(19)]. In the descloizite-type compounds (**1**, **2**), *M*2 atoms have site symmetry -1, while *M*1, *X*, O2, O3, O4, and H atoms have site symmetry *m*; only O1 is located on a general position. Both structure-types are characterized by slightly irregular $M2^{2+}O_4(OH)_2$ octahedrons that share O—OH edges to form infinite, weakly kinked chains parallel to [001] (Fig. 2). These chains are cross-linked by the

vertices of XO_4 to form a three-dimensional framework (Fig. 3). Voids in the framework are occupied by [7]- or [8]-coordinated $M1^{II}$ cations, for descloizite- and adelite-type members, respectively (Fig. 4).

The $M2^{2+}$ cations are [6]-coordinated to form $M2^{2+}O_4(OH)_2$ polyhedrons, the exact geometry of which depends on the character of the *M*2 atom. In the crystal structures of **1** and **4**, the *M*2 sites are occupied by Co^{2+}, and in **5** by Zn^{2+}. In these compounds the $M2^{2+}O_4(OH)_2$ polyhedrons are fairly regular octahedrons. In **2**, **3**, and **7**, the *M*2 position is occupied by Cu^{2+}. In minerals and synthetic inorganic solids, almost all $Cu\phi_6$ (ϕ: O^{2-}, OH^-, H_2O) octahedrons are strongly distorted away from holosymmetric symmetry owing to Jahn-Teller distortion. Usually, this distortion results in an axially elongated octahedron, designated as a [4 + 2] distortion. However, such a pattern of distortion is not always the case. There are a numerous examples where the $Cu\phi_6$ octahedron has two short bonds, two intermediate-length bonds, and two long bonds, i.e. a [2 + 2 + 2]-coordination (Burns and Hawthorne 1995). Such is the case in the structure of mottramite, $PbCu(OH)(VO_4)$ (Cooper and Hawthorne 1995); the intermediate-length bonds (2.102 Å) are very close to the mean of the long and short bonds (2.117 Å). The same applies for the compounds **2**, **5**, and **8**, where Cu^{2+} cations also show [2 + 2 + 2]-coordination (Table 5).

The average <*M*2–O> bond lengths are 2.085, 2.089, 2.104, 2.121, 2.132, and 2.139 Å for **1**-**5** and **8**, respectively. These values are in good agreement with the values 2.11, 2.08, and 2.10 Å for <Co–O>, <Cu–O>, and <Zn–O>, respectively, calculated as the sums of effective ionic radii of the Co^{2+} and O^{2-} ions for **1** and **4**, Cu^{2+} and O^{2-} ions for **2**, **5**, and **8**, and Zn^{2+} and O^{2-} ions for **4** (Shannon 1976). According to the formula $\Delta_{oct} = 1/6\ \Sigma[(d_i–d_m)/d_m]^2$ (Robinson et al. 1971, Fleet 1976), the bond-length distortions for the three *M*2 atoms are $4.23\cdot10^{-4}$, $5.57\cdot10^{-3}$, $8.15\cdot10^{-3}$, $2.79\cdot10^{-3}$, $4.56\cdot10^{-3}$, and $11.35\cdot10^{-3}$, for **1**-**6**, respectively. These values indicate only moderate distortions of the octahedral geometry. However, the

296 polyhedrons containing Co^{2+} and Zn^{2+} are less distorted than those of Cu^{2+} and show a less
297 pronounced dependence on mean bond lengths, due to the Jahn-Teller distortion of copper(II).

298 The shared edges O3—O4 (descloizite-type) and O1—O5 (adelite-type) in the infinite
299 chains have lengths of 2.765(5), 2.611(3), 2.857(4), 2.842(6) and 2.922(5) Å, for **1-5**,
300 respectively and 2.897(3) Å for **8**. Due to this connection, the angular distortion for the
301 $M2O_4(OH)_2$ polyhedron is moderate: $\sigma_{oct}^2 = 1/11\ \Sigma\ (\angle_i - 90)^2$ (Robinson et al. 1971, Fleet
302 1976) is 15.87, 29.76, 9.619, 16.193, and 18.431 for **1-5**, respectively and 23.927 for **8**. As
303 expected, the smallest O—*M*2—O angles occur in the case of shared edges between the
304 $M2O_4(OH)_2$ octahedrons (Table 5), while for the other O atoms in *cis*-arrangement the O—
305 *M*2—O angles are larger (Table 5).

306 The coordination figure around the X^{5+} cations (X = V, As) is a tetrahedron. The average
307 X—O bond lengths are: 1.688, 1.684, 1.695, 1.691, and 1.713 Å for **1-5**, respectively and
308 1.692 Å for **8** (Table 5). According to the formulae $DI(TO)_{tet} = (\Sigma|\ TO_i\text{-}TO_m\ |)/4TO_m$ and
309 $DI(OTO)_{tet} = (\Sigma|\ OTO_i\text{-}OTO_m\ |)/6OTO_m$ (Baur, 1974), distortion parameters for the X–O
310 distances, DI (TO) ($5.62\cdot10^{-3}$, $6.79\cdot10^{-3}$, $3.39\cdot10^{-3}$, $3.54\cdot10^{-3}$, and $18.53\cdot10^{-3}$ for **1-5**,
311 respectively and $7.53\cdot10^{-3}$ for **8**) and distortion parameters of the tetrahedral O–X–O angles,
312 DI(OTO) (0.027, 0.068, 0.031, 0.038, and 0.030 for **1-5**, respectively and 0.039 for **8**) are in
313 expected ranges: the longest X–O bonds are to the oxygen atom from the shared octahedral
314 edge (O3 and O1 in the descloizite- and adelite-type structures, respectively). The second
315 oxygen atom from this shared edge is the OH group (O4 and O5, respectively). The greatest
316 DI (TO) distortion is shown by the VO_4 tetrahedron in **5**. The distortion of the O—X—O
317 angles is only moderate and similar to that observed for other well-refined arsenates and
318 vanadates.

In the descloizite-type members (**1**-**2**), the *M*1 cations are [7]-coordinated to six oxygens and one OH group. Further oxygen atoms are at distances larger than 3.322(2) and 3.293(1) Å for **1** and **2**, respectively, indication only very weak bonding interactions. The [*M*1(OH)O_6] polyhedrons may be described as mono-capped trigonal prisms (Fig. 4a). The average <*M*1–O> bond lengths are 2.455 and 2.431 Å for **1** and **2**, respectively (for further *M*1–O bond lengths see Table 5). In the adelite-type members (**3**-**5** and **8**), the *M*1 cations are [8]-coordinated to seven oxygens and one OH group. The [*M*1(OH)O_7] polyhedrons may be described as bi-capped trigonal prisms, rather than square antiprisms (Fig. 4b). They are linked to each other via O3—O4 edges forming chains parallel to the *a*-axis and are further interconnected to a 3D framework by common O2 vertices. The average <*M*1–O> bond lengths are 2.618, 2.535, and 2.614 Å for **3**-**5**, respectively and 2.512 Å for **8** (for further interatomic bond lengths see Table 5).

The bond-valence sums of the anions (Table 6) are in the expected ranges and confirm the results of the structure refinement that O4/O5 forms the OH^- group and is a donor of a hydrogen-bond and O2 is the acceptor of a hydrogen-bond for the descloizite- (**1**-**2**) and adelite-type representatives (**3**-**5** and **8**), respectively. The hydrogen-bonds are of medium strong intensity (Table 5) with expected valence contributions between 0.17-0.27 valence units (v.u.). These are values sometimes far from the "necessary" ideal valence of 0.37 v.u. according to Table 6. Similar discrepancies among calculated bond-valence contributions ν were detected by Keller et al. (2003) for arsendescloizite, $PbZn(OH)(AsO_4)$ (O5···O2 = 2.806 Å, ν_{calc} = 0.18-0.20 v.u., $\nu_{H\text{-}bond}$ = 0.28-0.34) and by Clark et al. (1997) for austinite, $CaZn(OH)(AsO_4)$ (O5···O2 = 2.723 Å, ν_{calc} = 0.27-0.36, $\nu_{H\text{-}bond}$ = 0.21-0.24).

Raman spectroscopy

Raman spectra are shown in Figs. 5 and 6. They reflect the complexity of crystal structures. Bands in the high-energy range (2800–3800 cm^{-1}) are assigned to stretching of O–H bonds of hydroxyl groups. Bands in the 100–1200 cm^{-1} range are caused by either internal vibrations of XO_4 (X = As,V) tetrahedrons, or due to external vibrational modes.

Based on the d–ν correlation for hydrogen bonds (Libowitzky 1999), our Raman-shift values observed in the O–H stretching region (Fig. 5) are in very good agreement with the refined O–H···O bond lengths of 2.622(4) Å for **2** (Raman band obtained at 3051 cm^{-1}), 2.688(2) Å for **8** (3162 cm^{-1}), 2.670(6) Å for **1** (3217 cm^{-1}), 2.757(4) Å for **5** (3217 cm^{-1}), 2.680(5) Å for **4** (3300 cm^{-1}), and 2.766(3) Å for **3** (3345 cm^{-1}). Note that the main O–H band we detected for **8** (conichalcite; observed at 3162 cm^{-1}) is in very good agreement with the value of 3158 cm^{-1} described for natural conichalcite from the Lorena mine, Queensland, Australia (Martens et al. 2003). The fact that our OH band is narrower than that of Martens at al. (2003) is explained by the more irregular environment due to the minor presence of non-formula elements in the natural conichalcite specimen. All Raman spectra except that of **2** show additional minor bands in the O–H stretching region.

The range of O–H stretching values observed in the present study (Fig. 5) suggests that the type of *M*2 cation affects appreciably the spectral position of the hydroxyl stretching band(s), with smaller *M*2 cations tending to shift the O–H stretching bands to higher energy. Comparison of O–H stretching bands observed for **5** [$SrCu(OH)(VO_4)$; main signal at 3217 cm^{-1}] with O–H bands of mottramite, $PbCu(OH)(VO_4)$ (3548 and 3515 cm^{-1}; Frost et al. 2001) implies that the same seems to apply to the *M*1 cation, although the difference between the ionic radius of $^{[7]}Sr^{2+}$ and $^{[7]}Pb^{2+}$ (1.21 and 1.23 Å, respectively; Shannon 1976) is not very large.

Bands in the 700–1000 cm^{-1} range are assigned to symmetric and antisymmetric stretching modes of the $(XO_4)^{3-}$ groups, whereas internal bending vibrations of these tetrahedrons are observed at below 550 cm^{-1}, here partially overlaid by various external modes (Fig. 6). For all substances studied, the XO_4 stretching bands have quite similar Raman shifts (Fig. 6). The most intense Raman bands were observed at around 820 and 800 cm^{-1} for **3**, 818, 804, and 790 cm^{-1} for **4**, 823 and 797 cm^{-1} for **1**, 833 and 824 cm^{-1} for **8**, and for **2** at 834 and 809 cm^{-1}. These Raman-shift values are in excellent agreement with published data for the adelite-group minerals (Martens et al. 2003). For **5**, the $(VO_4)^{3-}$ stretching modes lie at around 840, 821, and 805 cm^{-1}; these values correlate very well with Raman-band values reported for the vanadate minerals descloizite and mottramite (Frost et al. 2001; compare also Grzechnik 1991).

Structural relations to other compounds

The structural relation between descloizite- and adelite-type compounds and comparable compounds (natrochalcite and brackebuschite supergroups, see below), where $M2O_6$ octahedrons (or tetragonal bipyramids) are edge-linked into chains connected by XO_4 tetrahedrons (or anion groups) into layers or into a three-dimensional network are obvious. In these structures the cavities house *M*1 atoms. The atomic ratio *M*1:*M*2 in these compounds is 1:1 (descloizite/adelite), 1:2 (natrochalcite supergroup group), and 2:1 (brackebuschite supergroup). It is remarkable that within these different topological types, coupled substitution schemes involving *M*1, *M*2, and *X* atoms with different valences are known, some of them requiring also a substitution $[(OH)]^- \leftrightarrow [O]^{2-}$ or $[H_2O]^0 \leftrightarrow [(OH)]^-$ for charge balance.

Structural similarities are proven for the natrochalcite supergroup of minerals and synthetic compounds. The general chemical formula of this group is

391 $M1M2_2(XO_4)_2(H_2O,OH)_2$, where $M1^{1+,2+,3+}$ = Na, K, Rb, Ag, NH_4, Ca, Pb, Bi, Tl; $M2^{2+,3+}$ =
392 Al, Mn^{3+}, Fe^{3+}, Co, Ni, Cu, Zn; $X^{5+,6+}$ = P, As, V, S, Se, Mo (Effenberger et al. 2000, Krause
393 et al. 2002a, Brugger et al. 2002, Mihajlović and Effenberger 2004, and references therein).
394 The $M2O_6$ polyhedrons are edge-connected into chains which are linked by XO_4 tetrahedrons
395 into layers. They are connected by $M1^{[6+2]}$, $M1^{[7]}$, or $M1^{[8]}$ atoms and by hydrogen bonds. For
396 each of the cation sites *M*1, *M*2, and *X* at least two different valences are possible; the coupled
397 substitution at these sites ensures electro-neutrality. Furthermore, charge balance is also
398 realised by adjusting the ratio $OH:H_2O$ or, in the case of $SrCo_2(AsO_4)(AsO_3OH)(OH)(H_2O)$
399 (Mihajlović and Effenberger 2004), by introduction of (partially) protonated arsenate groups.

400 The relation between the crystal structures of the descloizite-adelite and brackebuschite
401 groups was originally mentioned by Donaldson and Barnes (1955b). Detailed structural
402 investigations of individual members were performed by Abraham et al. (1978), Chopin et al.
403 (1993), Foley et al. (1997), and Cámara et al. (2014). The general formula of the
404 brackebuschite supergroup (monoclinic, $P2_1/m$) is $M1_2M2(XO_4)_2(H_2O,OH)$, where $M1 = Ca^{2+}$,
405 Sr^{2+}, Ba^{2+}, Pb^{2+}; $M2 = Al^{3+}$, Mn^{2+}, Mn^{3+}, Fe^{2+}, Fe^{3+}, Zn^{2+}; and $X = P^{5+}$, S^{6+}, V^{5+}, As^{5+}. The
406 topology of this group is characterized by octahedral chains decorated by XO_4 tetrahedrons.
407 The octahedrons share edges and house smaller *M*2 cations. The chains are linked by large
408 *M*1 cations into a three-dimensional framework. Four ligands bridge *M*2 cations to the
409 adjacent arsenate tetrahedrons giving the chains the resemblance of four-membered pinwheels
410 when viewed along the screw twofold axis. The chains are linked by two distinct *M*1-centered
411 polyhedrons.

412 The minerals adopting the general formula $Bi_2Fe^{3+}M(O,OH)_2(OH)_2(AsO_4)_2$, where *M* =
413 Fe^{3+} (neustädtelite) or Cu^{2+} (medenbachite) (Krause et al. 1996, 2002b), adopt an atomic
414 arrangement similar to that descloizite-adelite compounds. Trivalent *M* cations cause a ratio
415 O:OH of 2:2, whereas divalent *M* cations result in a O:OH ratio of 1:3. The charge-balancing

exchange mechanism is $[M^{2+}O(OH)]^{-} \leftrightarrow [M^{3+}O]$. The change of the O:OH ratio is responsible for extensive order-disorder phenomena observed for the Bi atoms (Krause et al. 2002b).

Crystal chemistry and the space-group symmetry

Among minerals, the descloizite-type representatives (*Pnam*) are mostly lead vanadates, whereas the calcium arsenates and silicates favor the acentric structure variant (adelite group, $P2_12_12_1$). All minerals and synthetic compounds with $M1$ = Ca crystallize in space group $P2_12_12_1$ and show [8]-coordination for the Ca atoms (Table 1). The majority of the minerals and synthetic compounds with $M1 = Pb^{2+}$ adopt space group *Pnam* and [7]-coordination for the Pb atoms. Pb^{2+} atoms have a $6s^2$ lone-electron pair, which might be stereo-chemically active or inactive. However, one-sided coordinations are preferred. In descloizite-type structures the [7]-coordination for Pb^{2+} cations (mono-capped trigonal prism) is favored, because of the one-sided arrangement (seventh ligand decorating one face of the trigonal prism) of the oxygens around the central atom. The steric activity of the lone-pair electrons in the case of $M1 = Pb^{2+}$ can, however, not be the single reason for the change of the coordination figure and space-group symmetry, because in two minerals with $M1 = Pb^{2+}$, duftite and arsendescloizite, Pb atoms are in [8]-coordination and adopt space-group symmetry $P2_12_12_1$. In the synthetic compounds with $M1 = Na^{+}$ and Cd^{2+}, where cations have completely filled electron shells, and where a regular coordination figure is expected, they are [7]-coordinated (Table 1).

With the exception of the $CdCo(OH)(AsO_4)$, $CdCu(OH)(AsO_4)$, and $HgZn(OH)(AsO_4)$, all other arsenates adopt the acentric adelite structure-type. In contrast, most vanadates of the descloizite supergroup adopt the descloizite structure-type. The exceptions are tangeite [$CaCu(OH)(VO_4)$], gottlobite [$CaMg(OH)((V,As)O_4)$], and

440 $SrCu(OH)(VO_4)$. In the structurally studied, Sr-, Pb-, and Mn-bearing tangeite sample (Basso
441 et al. 1989), the *X* site is occupied by both V and As in a 2:1 ratio, and in all these three
442 compounds M1 ≠ Pb^{2+}. Correlations between the space-group symmetry and cations at the *M*2
443 position are not obvious. The size of the ionic radii for *M*2 does not correlate with the space-
444 group symmetry of the members of adelite and descloizite-type compounds.

445 With the intention to study in more detail the precise mechanism that directs space-
446 group symmetry, we performed additional crystal-chemical calculations. These were done
447 using the programs TRANSTRU and COMPSTRU (Tasci et al. 2012) hosted by the Bilbao
448 Crystallographic Server (http://www.cryst.ehu.es).

449 Presently, and including the results of this present paper, 17 minerals and at least 5
450 additional, synthetic compounds belong to the adelite and descloizite groups (Table 1).
451 Unfortunately, a great number of these compounds have been reported with different cell
452 settings and atom names. In order to standardize the coordinate settings, and to allow easy
453 comparison between different structures, we have transformed all reported structure models
454 for the adelite- and descloizite-group compounds to a reference model that corresponds to the
455 set of coordinates determined by Effenberger et al. (2002) for the structure of the adelite,
456 $CaMg(OH)(AsO_4)$. Prior to this transformation, all descloizite-group members were
457 transformed to the lower-symmetry space group $P2_12_12_1$ using the program TRANSTRU
458 (Tasci et al. 2012). The corresponding unit-cell transformation matrices, translation matrices,
459 and renumbering schemes for the O atoms are given in Table 7 (note that after application of
460 the corresponding matrices, atom coordinates still have to be transformed to a reference site
461 by a symmetry operator of the $P2_12_12_1$ space group).

462 In order to analyze the structure distortions involved, the comparison of the parental,
463 centrosymmetric structure of descloizite (Hawthorne and Faggiani 1982) with the other
464 members of adelite and descloizite group were made using the program COMPSTRU (Tasci

et al. 2012). The program compares two structures that crystallize in the same space group and have atoms occupying the same Wyckoff positions. The difference between them is quantified by the degree of lattice distortion S and the measure of similarity Δ (Bergerhoff et al. 1999), which is zero in the case of complete coincidence. In addition, the maximum distance, d_{max} and the average distance, d_{av}, are calculated (Table 8). The maximum distance, d_{max}, gives the maximal displacement between the atomic positions of the paired atoms. The average distance, d_{av}, is defined as the average of the distances between the atomic positions of the paired atoms over the primitive unit cell. The relative atomic coordinates of the adelite- and descloizite-type compounds, and corresponding coordinates derived from the parental structure-type (input file for the COMPSTRU) are given as Supplementary Material, Table 1S.

The results of the above calculations show that the structural changes depend mostly on the average ionic radii $(r_{M1} + r_X)/2$ and $(r_{M2} + r_X)/2$, rather than on the ratio of ionic radii (r_{M1}/r_X) and (r_{M2}/r_X) (Figs. 7-10). A linear dependence with a moderately high correlation coefficient R was found for the degree of lattice distortion, S versus the average ionic radii of both $(r_{M1} + r_X)/2$ and $(r_{M2} + r_X)/2$ (Figs. 7-8) and the maximal distances between the paired atoms of the two structure types, d_{max}, versus the average ionic radii $(r_{M1} + r_X)/2$ (Fig. 7). For S vs. $(r_{M1} + r_X)/2$ the obtained linear function is $f = 0.012(2)–0.014(3)x$, $R = 0.758(7)$, for S vs. $(r_{M2} + r_X)/2$ the obtained linear function is $f = 0.101(14)–0.157(27)x$, $R = 796(7)$, and for d_{max} *vs*. $(r_{M1} + r_X)/2$, the calculated linear equation is $f = 1.938(283)–2.005(371)x$ with $R = 0.770(105)$. The degree of lattice distortion, S, varies from 0.0024 to 0.05 and is the smallest for čechite, $PbFe(VO_4)(OH)$ (Pertlik 1989), and other lead vanadates of the descloizite group and the largest for the adelite-type silicates mozartite, $CaMn(SiO_3OH)$ (Nyfeler et al. 1997), and vuagnatite, $CaAl(SiO_4)(OH)$ (McNear et al. 1976) (Table 7). These two minerals have small Si^{4+} cations on the X position, which may be the reason for the large distortion values.

The maximal displacement between the atomic positions of the paired atoms, d_{max}, varies from 0.064 to 0.672. The smallest value is observed for the lead vanadates of the descloizite group, and the largest one for hermannroseite, $CaCu(OH)(PO_4)$ (Schlüter et al. 2011), the only phosphate among adelite- and descloizite-group compounds.

The measures of similarity, Δ, vary from 0.012 to 0.111. As expected, the most similar to the parent structure of descloizite, $PbCu(OH)(VO_4)$, are the other lead vanadates of descloizite group, čechite and pyrobelonite, while the structure of duftite, $PbCu(OH)(AsO_4)$ (Kharisun et al. 1998), that instead of the large V^{5+} [$r(V^{5+})$ = 0.355 Å, Shannon 1976], contains the smaller As^{5+} [$r(As^{5+})$ = 0.335 Å] on the *X* position, is the least similar one.

In contrast, the correlations of *S*, Δ, d_{max}, and d_{av} with the ratio of the ionic radii, r_{M1}/r_X and r_{M2}/r_X are not linear (Figs. 9-10). The greatest lattice distortion, *S*, is as expected, observed for the silicates of the adelite group, and the smallest is again shown by the lead vanadates of the descloizite group. The least similar structure is again that of duftite (Fig. 8). The values for d_{max} and d_{av} are greatest for hermannroseite, and smallest for čechite, pyrobelonite, and mottramite (Figs. 9-10).

IMPLICATIONS

The crystal-chemistry of seven mineral-like samples synthesized within this study allows us to exclusively determine mechanisms controlling space-group symmetries among descloizite- and adelite-group compounds. We show that the presence of either relatively small Cd^{2+} or relatively big Sr^{2+} cations on the *M*1 position (in minerals mostly occupied by Pb^{2+} and Ca^{2+}) does not change the space-group symmetry. However, attempts to synthesise new group members with the fairly big Ba^{2+} cation on the *M*1 position were unsuccessful, indicating that the Ba^{2+} cation is too large for these structure types.

As results of the performed crystal-chemical calculations and evaluations, the following implications emerged: the mechanisms controlling space-group symmetries among descloizite- and adelite-group compounds are based on the ratio of space requirements of the atoms on the *M*1 and *X* sites. The calculations also showed that the discrete structural changes compared to the parental structure of the mineral descloizite depend mostly on the average ionic radii $(r_{M1} + r_X)/2$ and $(r_{M2} + r_X)/2$, rather than on the ratio of ionic radii (r_{M1}/r_X) or (r_{M2}/r_X). The influence of the stereochemically active lone-electron pairs on the change of the space-group symmetry from *Pnam* to $P2_12_12_1$ is rather small, an observation which is strengthened by the structural characterization of four synthetic descloizite-type members with seven-coordinated Cd^{2+} (having a completely filled electron shell) on the *M*1 position.

ACKNOWLEDGEMENTS

Financial support by the Austrian Science Foundation (FWF) (Grant V203-N19) is gratefully acknowledged. The lead author is thankful to Prof. Herta Effenberger for awakening the interest in descloizite- and adelite-group compounds. The EPMA measurements were done with the help of Franz Kiraly. Thomas Pippinger assisted with the Stoe StadiVari measurements and Maurizio Dini is thanked for providing the conichalcite specimen for investigation. The reviewer M. E. Ciriotti and two anonymous reviewers are thanked for their careful corrections and comments which helped to improve the manuscript.

REFERENCES

Abraham, K., Kautz, K., Tillmanns, E., and Walenta, K. (1978) Arsenbrackebuschite, $Pb_2(Fe,Zn)(OH,H_2O)[AsO_4]_2$, a new arsenate mineral. Neues Jahrbuch für Mineralogie, Monatshefte, 1978, 193-196.

538 Altomare, A., Burla, M.C., Camalli, M., Cascarano, G.L., Giacovazzo, C., Guagliardi, A.,
539 Moliterni, A.G.G., Polidori, G., and Spagna, R. (1999) *SIR*97: a new tool for crystal
540 structure determination and refinement. Journal of Applied Crystallography, 32, 115-
541 119.

542 Bachmann, H.G. (1953a) Die Kristallstruktur des Descloizit. Acta Crystallographica, 6, 102
543 (in German).

544 Bachmann, H.G. (1953a) Beitrag zur Kristallchemie natürlicher und künstlicher
545 Schwermetallvanadate. II. Die Kristallstruktur des Descloizit. Neues Jahrbuch für
546 Mineralogie, Monatshefte, 1953, 193-208 (in German).

547 Barnes, W.H. and Ahmed, F.R. (1969) A note on the unit cell constants, and X-ray diffraction
548 powder pattern, of pyrobelonite. Canadian Mineralogist, 10, 117-123.

549 Basso, R., Palenzona, A., and Zefiro, L. (1989) Crystal structure refinement of a Sr-bearing
550 term related to copper vanadates and arsenates of adelite and descloizite groups. Neues
551 Jahrbuch für Mineralogie, Monatshefte, 1989, 300-308.

552 Basso, R., Lucchetti, G., Zefiro, L., and Palenzona, A. (1993) Mozartite, $CaMn(OH)SiO_4$, a
553 new mineral species from the Cerchiara mine, northern Apennines, Italy. Canadian
554 Mineralogist, 31, 331-336.

555 Basso, R., and Zefiro, L. (1994) Mineral nomenclature: status of calciovolborthite and
556 tangeite. Neues Jahrbuch für Mineralogie, Monatshefte, 1994, 205-208.

557 Baur, W.H. (1974) The geometry of polyhedral distortions. Predictive relationships for the
558 phosphate group. Acta Crystallographica, B30, 1195□1215.

559 Bergerhoff, G., Berndt, M., Brandenburg, K., and Degen, T. (1999) Concerning inorganic
560 crystal structure types. Acta Crystallographica, B55, 147-156.

561 Brese, N.E. and O'Keeffe, M. (1991) Bond-valence parameters for solids. Acta
562 Crystallographica, B47, 192-197.

Brugger, J., Krivovichev, S., Kolitsch, U., Meisser, N., Andrut, M., Ansermet, S., and Burns, P.C. (2002) Description and crystal structure of manganlotharmeyerite, $Ca(Mn^{3+},\square,Mg)_2\{AsO_4,[AsO_2(OH)_2]\}_2(OH,H_2O)_2$, from the Starlera Mn deposit, Swiss Alps, and a redefinition of lotharmeyerite. Canadian Mineralogist, 40, 1597-1608.

Burns, P.C. and Hawthorne, F.C. (1995) Coordination geometry structural pathways in Cu^{2+} oxysalt minerals. Canadian Mineralogist, 33, 889-905.

Cámara, F., Ciriotti, M.E., Bittarello, E., Nestola, F., Massimi, F., Radica, F., Costa, E., Benna, P., and Piccoli, G.C. (2014) As-bearing new mineral species from Valletta mine, Maira Valley, Piedmont, Italy: I. Grandaite, $Sr_2Al(AsO_4)_2(OH)$, description and crystal structure. Mineralogical Magazine, 78, 757-774.

Cesbron, F., Ginderow, D., Giraud, R., Pelisson, P., and Pillard, F. (1987) La nickelaustinite, $Ca(Ni,Zn)(AsO_4)(OH)$: Nouvelle espece minerale du district Cobalto-Nickelifere de Bou-Azzer, Maroc. Canadian Mineralogist, 25, 401-407 (in French).

Chopin, C., Brunet, F., Gebert, W., Medenbach, O., and Tillmanns, E. (1993) Bearthite, $Ca_2Al(PO_4)_2(OH)$, a new mineral from high-pressure terrane of the western Alps. Schweizerische Mineralogische und Petrographische Mitteilungen, 73, 1-9.

Clark, L.A., Pluth, J.J., Steele, I., Smith, J.V., and Sutton, S.R. (1997) Crystal structure of austinite, $CaZn(AsO_4)OH$. Mineralogical Magazine, 61, 677-693.

Clearfield, A., Gopal, R., and Saldarriaga-Molina, C.H. (1977) Studies in heavy-metal molybdates. 2. Crystal structure of di-μ-hydroxo-dizinc(II) molybdate. Inorganic Chemistry, 16, 628-631.

Cooper, M.A. and Hawthorne, F.C. (1995) The crystal structure of mottramite, and the nature of Cu Zn solid solution in the mottramite-descloizite series. Canadian Mineralogist, 33, 1119-1124.

588 Donaldson, D.M. and Barnes, W.H. (1955a) The structures of the minerals of the descloizite
589 and adelite groups: II - pyrobelonite. American Mineralogist, 40, 580-596.

590 Donaldson, D.M. and Barnes, W.H. (1955b) The structures of the minerals of the descloizite
591 and adelite groups: III - brackebuschite. American Mineralogist, 40, 597-613.

592 Đorđević, T. (2007): Five new members of adelite- and descloizite-structure type. MinPet
593 2007, Meran, Italy, September 16-21, 2007, Mitteilungen der Österreichischen
594 Mineralogischen Gesellschaft, 153, 40 (abs.).

595 Đorđević, T. (2008a) Barium zinc diarsenate. Acta Crystallographica, E64, i57.

596 Đorđević, T. (2008b) $BaCo_2(AsO_4)_2$. Acta Crystallographica, E64, i58-i59.

597 Đorđević, T. (2010) $Zn_{1.86}Cd_{0.14}(OH)VO_4$. Acta Crystallographica, E66, i79.

598 Đorđević, T. (2011) $Ba(ZnAsO_4)_2{\cdot}H_2O$, a non-centrosymmetric framework structure related to
599 feldspar. European Journal of Mineralogy, 23, 437-447.

600 Đorđević, T. and Karanović, Lj. (2008) Synthesis, crystal structure, infrared and Raman
601 spectra of $Sr_4Cu_3(AsO_4)_2(AsO_3OH)_4{\cdot}3H_2O$ and $Ba_2Cu_4(AsO_4)_2(AsO_3OH)_3$. Journal of
602 Solid State Chemistry, 181, 2889-2898.

603 Đorđević, T. and Karanović, Lj. (2010) A new polymorph of $Ba(AsO_3OH)$: synthesis, crystal
604 structure and vibrational spectra. Journal of Solid State Chemistry, 183, 2835-2844.

605 Đorđević, T. and Karanović, Lj. (2013) $Ba[Co_3(VO_4)_2(OH)_2]$ with a regular Kagomé lattice.
606 Acta Crystallographica, C69, 114-118.

607 Đorđević, T. and Kolitsch, U. (2008) Conichalcite revisited: Structural and chemical
608 characterisation of a sample from the Maria Catalina mine, Copiapó Province, Chile.
609 Annual Meeting of the DMG, Berlin, Germany, September 14-17, 2008; CD with
610 abstracts, Abs. no. 331.

611 Đorđević, T. and Kolitsch, U. (2013) Five-coordinate Cd in the crystal structure of triploidite-
612 type $Cd_2(AsO_4)(OH)$. Mineralalogy and Petrology, 107, 243-251.

Đorđević, T., Karanović, Lj., and Tillmanns, E. (2008a) $Mg_{13.4}(OH)_6(HVO_4)_2(H_{0.2}VO_4)_6$: structural and spectroscopic study. Crystal Research and Technology, 43, 1202-1209.

Đordević, T., Stojanović, J., Šutović, S., and Karanović, Lj. (2008b) Sr-, Ba- and Cd-arsenates with the apatite-type structure. Acta Crystallographica, C64, i82-i86.

Đorđević, T., Wittwer, A., and Krivovichev, S.V. (2015) Three new alluaudite-like protonated arsenates: $NaMg_3(AsO_4)(AsO_3OH)_2$, $NaZn_3(AsO_4)(AsO_3OH)_2$ and $Na(Na_{0.6}Zn_{0.4})Zn_2(H_{0.6}AsO_4)(AsO_3OH)_2$. European Journal of Mineralogy, 27, 559-573.

Dowty, E. (2000) ATOMS for Windows V. 6.3. Shape Software, Kingsport, Tennessee, USA.

Dunn, P.J. (1983) Pyrobelonite from Franklin, New Jersey. Mineralogical Record, 14, 203-204.

Effenberger, H. (1988) On the crystal chemistry of three copper(II)-arsenates: $Cu_3(AsO_4)_2$-III, $Na_4Cu(AsO_4)_2$, and $KCu_4(AsO_4)_3$. Monatshefte für Chemie, 119, 1103-1112.

Effenberger, H. (2002) $CdCu(OH)(AsO_4)$, the first Cd member of the adelite-descloizite structure type. Zeitschrift für Kristallographie, Supplement Issue, 19, 85.

Effenberger, H. and Pertlik, F. (1988) Comparison of the homeomorphic crystal structures of $Pb(Fe,Mn)(VO_4)(OH)$ = čechite and $PbCu(AsO_4)(OH)$ = duftite. Zeitschrift für Kristallographie, 185, 610.

Effenberger, H., Krause, W., Bernhardt, H.-J., and Martin, M. (2000) On the symmetry of tsumcorite group minerals based on the new species rappoldite and zincgartrellite. Mineralogical Magazine, 64, 1109-1126.

Effenberger, H., Krause, W., and Bernhardt, H.J. (2002) Structural investigations of adelite and cobaltaustinite, two members of the adelite-descloizite group. EMPG IX Meeting, Zürich, Switzerland, Journal of Conference Abstracts, 7, 30.

England, B.M. and Robinson, N. (1988) Mimetite and duftite from the Mount Bonnie Mine, Northern Territory. Mineralogical Record, 19, 441-450.

638 Farrugia, L.J. (2012) *WinGX* and *ORTEP for Windows*: an update. Journal of Applied
639 Crystallography, 45, 849-854.

640 Ferraris, G. and Ivaldi, G. (1988) Bond valence vs bond length in O···O hydrogen bonds. Acta
641 Crystallographica, B44, 341-344.

642 Flack, H.D. (1983) On enantiomorph-polarity estimation. Acta Crystallographica, A39, 876.

643 Fleet, M.E. (1976) Distortion parameters for coordination polyhedra. Mineralogical Magazine,
644 40, 531-533.

645 Foley, J.A., Hughes, J.M., and Lange, D. (1997) The atomic arrangement of brackebuschite,
646 redefined as $Pb_2(Mn^{3+},Fe^{3+})(VO_4)_2(OH)$, and comments on Mn^{3+} octahedra. Canadian
647 Mineralogist, 35, 1027-1033.

648 Frost, R.L., Williams, P.A., Kloprogge, J.T., and Leverett, P. (2001) Raman spectroscopy of
649 descloizite and mottramite at 298 and 77 K. Journal of Raman Spectroscopy, 32, 906-
650 911.

651 Giuseppetti, G. and Tadini, C. (1988) The crystal structure of austinite, $CaZn(AsO_4)(OH)$
652 from Kamareza, Laurion (Greece). Neues Jahrbuch für Mineralogie. Monatshefte,
653 1988, 159-166.

654 Gołębiowska, B., Pieczka, A., and Franus, W. (1988) Conicalcite, clinotyrolite and tyrolite
655 (Ca-Cu arsenates) from Rędziny (Lower Silesi, Poland). Mineralogica Polonica, 29,
656 13-22.

657 Grzechnik, A. (1991) Evaluation of the V–O stretching and V–O bond-bond interaction force
658 constants of the VO_4^{3-} ions in the structure of descloizite, $PbZn(VO_4(OH)$. Neues
659 Jahrbuch für Mineralogie Monatshefte, 1991, 465-472.

660 Guillemin, G. (1956) Contribution à la minéralogie des arséniates, phosphates et vanadates de
661 cuivre. I. Arséniates. Bulletin de la Société française de Minéralogie et de
662 Cristallographie, 79, 7-95 (in French).

663 Hawthorne, F.C. and Faggiani, R. (1979) Refinement of the structure of descloizite. Acta
664 Crystallographica, B35, 717-720.

665 Healey, A.M., Weller M.T., and Genge, A.R. (1999) Synthesis and structure of $NaZnSiO_3OH$,
666 a new chiral zincosilicate framework material. Inorganic Chemistry, 38, 455-458.

667 Henderson, R.R., Yang, H., Downs, R.T., and Jenkins, R.A. (2008) Redetermination of
668 conichalcite, $CaCu(AsO_4)(OH)$. Acta Crystallographica, E64, i53-i54.

669 Hill, J.R. (1976) The crystal structure and infrared properties of adamite. American
670 Mineralogist, 61, 979-986.

671 Keller, P. and Dunn, P.J. (1982) Arsendescloizite, a new mineral from Tsumeb. Mineralogical
672 Record, 13, 155-157.

673 Keller, P., Lissner, F., and Schleid, T. (2003) The crystal structure of arsenodescloizite.
674 $PbZn(OH)[AsO_4]$, from Tsumeb (Namibia). Neues Jahrbuch für Mineralogie,
675 Monatshefte, 2003, 374-384.

676 Kharisun, Taylor, M.R., and Bevan, D.J.M. (1998) The crystal chemistry of duftite,
677 $PbCu(AsO_4)OH$ and the β-duftite problem. Mineralogical Magazine, 62, 121-130.

678 Kolitsch, U. (2001) Refinement of pyrobelonite, $PbMn^{II}VO_4(OH)$, a member of the
679 descloizite group. Acta Crystallographica, E57, i119-i121.

680 Kovač, S., Karanović, Lj., and Đorđević, T. (2015) An investigation of polyhedral
681 deformation in two mixed-metal diarsenates: $SrZnAs_2O_7$ and $BaCuAs_2O_7$. Acta
682 Crystallographica, C71, 330-337.

683 Krause, W., Bernhardt, H.-J., Gebert, W., Graetsch, H., Belendorff, K., and Petitjean, K.
684 (1996) Medenbachite, $Bi_2Fe(Cu,Fe)(O,OH)_2(OH)_2(AsO_4)_2$, a new mineral species: its
685 description and crystal structure. American Mineralogist, 81, 505-512.

686 Krause, W., Bernhardt, H.-J., Effenberger, H., and Witzke, T. (2002a) Schneebergite and
687 nickelschneebergite from Schneeberg, Saxony, Germany: The first Bi-bearing
688 members of the tsumcorite group. European Journal of Mineralogy, 14, 115-126.

689 Krause, W., Bernhardt, H.-J., McCammon, C., and Effenberger, H. (2002b) Neustädtelite and
690 cobaltneustädtelite, the Fe^{3+}- and Co^{2+}-analogues of medenbachite. American
691 Mineralogist, 87, 726-738.

692 Leistner, H. and Chatterjee, N.D. (1978) Water-containing minerals in the $CaSiO_3$- Al_2O_3--
693 H_2O system: rosenhahnite $Ca_3[Si_3O_8(OH)_2]$, vuagnatite $CaAl[SiO_4](OH)$ and
694 chantalite $CaAl_2SiO_4(OH)_4$. Fortschritte der Mineralogie, Beiheft, 56, 79-80 (in
695 German).

696 Libowitzky, E. (1999) Correlation of O—H stretching frequencies and O—H···O hydrogen
697 bond lengths in minerals. Monatshefte für Chemie, 130, 1047-1059.

698 Marsh, R.E. and Schomaker, V. (1979) Some incorrect space groups in Inorganic Chemistry.
699 Inorganic Chemistry, 18, 2331-2336.

700 Martens, W., Frost, R.L., and Williams, P.A. (2003) Molecular structure of the adelite group
701 of minerals - a Raman spectroscopic study. Journal of Raman Spectroscopy, 34, 104-
702 111.

703 McNear, E., Vincent, M.G., and Parthé, E. (1976) The crystal structure of vuagnatite,
704 $CaAl(OH)(SiO_4)$. American Mineralogist, 61, 831-838.

705 Mihajlović, T. and Effenberger, H. (2004) The first proof of protonated anion tetrahedra in the
706 tsumcorite-type compounds. Mineralogical Magazine, 68, 757-767.

Mihajlović, T. and Effenberger, H. (2006) Synthesis and crystal structure of $Sr(AsO_3OH)$ and $Ba(AsO_3OH)$: crystal chemistry of related $MHXO_4$ (X = As, P, S) compounds. Zeitschrift für Kristallographie, 221, 770-781.

Mihajlović, T., Libowitzky, E., and Effenberger, H. (2004a) Synthesis, crystal structure, Raman and infrared spectra of $Sr_5(As_2O_7)_2(AsO_3OH)$. Journal of Solid State Chemistry, 177, 3963-3970.

Mihajlović, T., Kolitsch, U., and Effenberger, H. (2004b) $BaMgAs_2O_7$ and $BaCoAs_2O_7$ – synthesis, crystal structures and twinning of two new barium diarsenates. Journal of Alloys and Compounds, 379, 103-109.

Mills, S.J., Hatert, F., Nickel, E.H., Ferraris, G. (2009): The standardisation of mineral group hierarchies: application to recent nomenclature proposals. European Journal of Mineralogy, 21, 1073-1080.

Moini, A., Peascoe, R., Rudolf, P.R., and Clearfield, A. (1986) Hydrothermal synthesis of copper molybdates. Inorganic Chemistry, 25, 3782-3785.

Moore, P.B. (1967) Gabrielsonite, $PbFe(AsO_4)(OH)$, a new member of the descloizite-pyrobelonite group, from Långban. Arkiv för Mineralogi Och Geologi, 4, 401-405.

Mrázek, Z. and Táborský, Z. (1981) Čechite, $Pb(Fe^{2+},Mn^{2+})(VO_4)(OH)$, a new mineral of the descloizite-pyrobelonite group. Neues Jahrbuch für Mineralogie, Monatshefte, 1981, 520-528.

Nickel, E.H. and Birch, W.D. (1988) Cobaltaustinite - a new arsenate mineral from Dome Rock, South Australia. American Mineralogist, 3, 53-57.

Nonius (2005-2007) COLLECT data collection software. Nonius BV, Delft, The Netherlands.

Nyfeler, D., Hoffmann, C., Armbruster, T., Kunz, M., and Libowitzky, E. (1997) Orthorhombic Jahn-Teller distortion and Si–OH in mozartite, $CaMn^{3+}O[SiO_3OH]$: A

single-crystal X-ray, FTIR, and structure modeling study. American Mineralogist, 82, 841-848.

Otwinowski, Z., Borek, D., Majewski, W., and Minor, W. (2003) Multiparametric scaling of diffraction intensities. Acta Crystallographica, A59, 228-234.

Permer, L., Laligant, Y., and Ferey, G. (1993) Crystal structure of $(Pb_{2.8}Fe_{1.2})Cu_4O_{1.6}(VO_4)_4(OH)_2$: structural relationships with mineral gamagarite. European Journal of Solid State and Inorganic Chemistry, 30, 383-392.

Pertlik, F. (1989) The crystal structure of čechite, $Pb(Fe^{2+}, Mn^{2+})(VO_4)(OH)$ with Fe > Mn. A mineral of the descloizite group. Neues Jahrbuch für Mineralogie, Monatshefte, 1989, 34-40.

Pring, A., Francis, G.L., and Birch, W.D. (1989) Pyrobelonite, arsenoklasite, switzerite and other recent finds at Iron Monarch, South Australia. Australian Mineralogist, 4, 49-55.

Qurashi, M.M. and Barnes, W.H. (1963) The structures of the minerals of the descloizite and adelite groups. IV: Descloizite and conichalcite (part 2). The structure of conichalcite. Canadian Mineralogist, 7, 561-577.

Qurashi, M.M. and Barnes, W.H. (1964) The structures of the minerals of the descloizite and adelite group. IV: Descloizite and conichalcite (part 3). Canadian Mineralogist, 8, 23-29.

Radcliffe, D. and Simmons, W.B., Jr. (1971) Austinite: chemical and physical properties in relation to conichalcite. American Mineralogist, 56, 1359-1365.

Robinson, K., Gibbs, G.V., and Ribbe, P.H. (1971) Quadratic elongation: a quantitative measure of distortion in coordination polyhedra. Science, 172, 567–570.

753 Rodnova, V.I. (1993) A rare finding of pyrobelonite in the iron-manganese ores of Atasu
754 deposit (central Kazakhstan). Proceedings of the Russian Mineralogical Society, 122,
755 62-65 (in Russian with English abstract).

756 Sakai, S., Yoshiasa, A., Sugiyama, K., and Miyawaki, R. (2009) Crystal structure and
757 chemistry of conichalcite, $CaCu(AsO_4)(OH)$. Journal of Mineralogical and
758 Petrological Sciences, 104, 125-131.

759 Sarp, H., Bertrand, J, and McNear, E. (1976) Vuagnatite, $CaAl(OH)SiO_4$, a new natural
760 calcium aluminum silicate. American Mineralogist, 61, 825-830.

761 Schlüter, J., Pohl, D., and Gebhard, G. (2011) The new mineral hermannroseite,
762 $CaCu(PO_4,AsO_4)(OH)$, the phosphate analogue of conichalcite, from Tsumeb,
763 Namibia. Journal of Mineralogy and Geochemistry, 188, 135-140.

764 Shannon, R.D. (1976) Revised effective ionic radii and systematic studies of interatomic
765 distances in halides and chalcogenides. Acta Crystallographica, A32, 751-767.

766 Sheldrick, G. (2008) A short history of *SHELX*. Acta Crystallographica, A64, 112–122.

767 Sokolova, E.V., Egorov-Tismenko, Yu.K., and Yakhontova, L.K. (1982) Study of crystalline
768 structures of rare arsenates: duftite and mimetite. Vestnik Moskovskogo Universiteta,
769 Geologiya, 37, 49-54.

770 Sokolova, E.V., Egorov-Tismenko, Yu.K., Simonov, M.A., and Krasnenko, T.I. (1986)
771 Refined crystal structure of the synthetic vanadate $Cd_2(V_2O_7)$. Soviet Physics -
772 Crystallography, 31, 722-723.

773 Stojanović, J., Đorđević, T., and Karanović, Lj. (2012) Structural features of two novel
774 alluaudite-like arsenates $Cd_{1.16}Zn_{2.34}(AsO_4)_{1.5}(HAsO_4)(H_2AsO_4)_{0.5}$ and
775 $Cd_{0.74}Mg_{2.76}(AsO_4)_{1.5}(HAsO_4)(H_2AsO_4)_{0.5}$. Journal of Alloys and Compounds, 520,
776 180-189.

777 Taggart, J.E. and Foord, E.E. (1980) Conichalcite, cuprian austinite, and plumbian
778 conichalcite from La Plata Country, Colorado. Mineralogical Record, 11, 37-38.

779 Tasci, E.S., de la Flor, G., Orobengoa, D., Capillas, C., Perez-Mato, J.M., and Aroyo, M.I.
780 (2012) An introduction to the tools hosted in the Bilbao Crystallographic Server. EPJ
781 Web of Conferences, 22, 00009.

782 van der Westhuizen, W.A., de Bruiyn, H., Tordiffe, E.A.W., and Botha, B.J.V. (1986) The
783 descloizite-mottramite series of vanadates from Otavi Mountain Land, South West
784 Africa: an X-ray study. Mineralogical Magazine, 50, 137-140.

785 Weil, M. (2004) $ZnHg(AsO_4)(OH)$ with a descloizite-type structure. Acta Crystallographica,
786 E60, i25-i27.

787 Weil, M., Đorđević, T., Lengauer, C.L., and Kolitsch, U. (2009) Investigations in the systems
788 Sr–As–O–*X* (*X*= H, Cl): Preparation and crystal structure refinements of the anhydrous
789 arsenates(V) $Sr_3(AsO_4)_2$, $Sr_2As_2O_7$, α- and β-$SrAs_2O_6$, and of the apatite-type phases
790 $Sr_5(AsO_4)_3OH$ and $Sr_5(AsO_4)_3Cl$. Solid State Science, 11, 2111-2117.

791 Witzke, Th., Steins, M., Doering, Th., and Kolitsch, U. (2000) Gottlobite,
792 $CaMg(VO_4,AsO_4)(OH)$, a new mineral from Friedrichroda, Thuringia, Germany.
793 Neues Jahrbuch für Mineralogie, Monatshefte, 2000, 444-454.

794 Yang, H., Costin, G., Keogh, J., Lu, R., and Downs, R.T. (2007) Cobaltaustinite,
795 $CaCo(AsO_4)(OH)$. Acta Crystallographica, E63, i53-i55.

796 Yang, H., Jenkins, R.A., Downs, R.T., Evans, S.H., and Tait, K.T. (2011) Rruffite,
797 $Ca_2Cu(AsO_4)_2{\cdot}2H_2O$, a new member of the roselite group, from Tierra Amarilla, Chile.
798 Canadian Mineralogist, 49, 877-884.

799 Zhao, B. (1985) Arsendescloizite discovered for the first time in China. Acta Mineralogica
800 Sinica, 5, 282-284 (in Chinese with English abstract).

FIGURE CAPTIONS

FIGURE 1. Back-scattered electrons image of the conichalcite sample from the Maria Catalina mine, showing intense, narrow growth zoning.

FIGURE 2. Crystal structures of (a) descloizite- and (b) adelite-type compounds in a view along the [001] direction. Representatives depicted are $CdCo(OH)(AsO_4)$ (a) and $SrCo(OH)(AsO_4)$ (b).

FIGURE 3. Crystal structures of (a) descloizite-and (b) adelite-type compounds in a view along the [010] direction. Representatives depicted are $CdCo(OH)(AsO_4)$ (a) and $SrCo(OH)(AsO_4)$ (b).

FIGURE 4. Sketches of the coordination figures around *M*1 cations in (a) descloizite- and (b) adelite-type compounds.

FIGURE 5. Plot of Raman spectra of **1** – **5** and **8**, showing the O–H stretching region. Spectra are presented with vertical offset for more clarity.

FIGURE 6. Plot of Raman spectra (stacked) of **1** – **5** and **8**, showing the lower-energy spectral range 100–1200 cm^{-1}.

FIGURE 7. Plots of the degree of lattice distortion, S, structure similarity, Δ, maximal displacement between the atomic positions of the paired atoms, d_{max}, and the average displacement between the atomic positions of the paired atoms, d_{av}, versus the average ionic radii $(r_{M1} + r_X)/2$. Squares = descloizite-group members; circles = adelite-group members. For abbreviations and references see Table 8.

FIGURE 8. Plots of the degree of lattice distortion, S, structure similarity, Δ, maximal displacement between the atomic positions of the paired atoms, d_{max}, and the average displacement between the atomic positions of the paired atoms, d_{av}, versus the average ionic radii $(r_{M2} + r_X)/2$. Squares = descloizite-group members; circles = adelite-group members. For abbreviations and references see Table 8.

FIGURE 9. Plots of the degree of lattice distortion, S, structure similarity, Δ, maximal displacement between the atomic positions of the paired atoms, d_{max}, and the average displacement between the atomic positions of the paired atoms, d_{av}, versus the ratio of ionic radii r_X/r_{M1}. Squares = descloizite-group members; circles = adelite-group members. For abbreviations and references see Table 8.

FIGURE 10. Plots of the degree of lattice distortion, S, structure similarity, Δ, maximal displacement between the atomic positions of the paired atoms, d_{max}, and the average displacement between the atomic positions of the paired atoms, d_{av}, versus the ratio of ionic radii r_X/r_{M2}. Squares = descloizite-group members; circles = adelite-group members. For abbreviations and references see Table 8.

Revision 1:

Table 1. Minerals and synthetic compounds belonging to the adelite and descloizite structure-types. The crystal data given in table were taken from the references marked with an asterisk (*).

Name	Composition	Space group	*a* (Å)	*b* (Å)	*c* (Å)	*V* (Å^3)	Reference
			Adelite structure type				
Vuagnatite	$Ca^{[8]}Al(OH)(SiO_4)$	$P2_12_12_1$	7.055(6)	8.542(7)	5.683(5)	342.5(5)	Sarp et al. (1976), McNear et al. (1976)*, Leistner and Chatterjee (1978)
Mozartite	$Ca^{[8]}Mn^{3+}O(SiO_3OH)$	$P2_12_12_1$	5.838(1)	7.224(1)	8.690(1)	366.5	Basso et al. (1993)*, Nyfeler et al. (1997)
Hermannroseite	$Ca^{[8]}Cu(PO_4,AsO_4)(OH)$	$P2_12_12_1$	7.328(7)	9.123(7)	5.769(6)	385.7(6)	Schlüter et al. (2011)
Nickelaustinite	$Ca^{[8]}(Ni,Zn)(OH)(AsO_4)$	$P2_12_12_1$	7.455(3)	8.955(3)	5.916(2)	395	Cesbron et al. (1987)
Cobaltaustinite	$Ca^{[8]}(Co,Cu^{2+})(OH)(AsO_4)$	$P2_12_12_1$	7.4919(9)	8.9946(9)	5.9158(7)	398.65(8)	Nickel and Birch (1988), Effenberger et al. (2002), Yang et al. (2007)*
Adelite	$Ca^{[8]}Mg(OH)(AsO_4)$	$P2_12_12_1$	7.468(1)	8.953(2)	5.941(1)	397	Effenberger et al. (2002)
Conichalcite	$Ca^{[8]}Cu(OH)(AsO_4)$	$P2_12_12_1$	7.4040(15)	9.2410(18)	5.8310(12)	398.96(14)	Qurashi and Barnes (1963), Taggart and Foord (1980), Gołębiowska et al. (1998), Đorđević and Kolitsch (2008), Henderson et al. (2008), Sakai et al. (2009), this work*
Gottlobite	$Ca^{[8]}Mg(OH)[(V,As)O_4]$	$P2_12_12_1$	7.501(4)	9.010(7)	398.96(14)	401.5(3)	Witzke et al. (2000)*
Austinite	$Ca^{[8]}Zn(OH)(AsO_4)$	$P2_12_12_1$	7.5092(8)	9.0438(9)	5.9343(8)	403	Radcliffe and Simmons (1971), Giuseppetti and Tadini (1988), Clark et al. (1997)*
Tangeite	$Ca^{[8]}Cu(OH)(VO_4)$	$P2_12_12_1$	5.836(1)	7.430(2)	9.347(1)	405	Basso et al. (1989*, 1994)
Gabrielsonite	$PbFe^{2+}(OH)(VO_4)$	$P2_1am$ (?)	7.86(1)	5.98(1)	8.62(1)	405	Moore (1967)
Duftite	$Pb^{[8]}Cu(OH)(AsO_4)$	$P2_12_12_1$	7.768(1)	9.211(1)	5.999(1)	429	Sokolova et al. (1982), England and Robinson (1988), Kharisun et al. (1998)*

Arsendescloizite	$Pb^{[8]}Zn(OH)(AsO_4)$	$P2_12_12_1$	7.646(2)	9.363(2)	6.077(1)	435	Zhao (1985), Keller and Dunn (1982), Keller et al. (2003)*
synthetic	$NaZn^{[4]}(SiO_3OH)$**	$P2_12_12_1$	7.6872(2)	9.3899(2)	5.155(1)	369.7(1)	Healey et al. (1999)
synthetic	$Sr^{[8]}Co(OH)(AsO_4)$	$P2_12_12_1$	7.608(2)	9.239(2)	6.027(1)	423.64(16)	this work
synthetic	$Sr^{[8]}Zn(OH)(AsO_4)$	$P2_12_12_1$	7.645(1)	9.263(2)	6.030(1)	427.04(14)	this work
synthetic	$Sr^{[8]}Cu(OH)(VO_4)$	$P2_12_12_1$	7.573(2)	9.639(2)	5.886(1)	429.66(16)	this work
			Descloizite structure type				
Mottramite	$Pb^{[7]}Cu(OH)(VO_4)$	*Pnma*	7.667(4)	6.053(2)	9.316(4)	432.3(3)	van der Westhuizen et al. (1986), Cooper and Hawthorne (1995)*
Descloizite	$Pb^{[7]}Zn(OH)(VO_4)$	*Pnma*	7.610(2)	6.047(2)	9.453(2)	435	Bachmann (1953a,b), Qurashi and Barnes (1964), Hawthorne and Faggiani (1979)*, Grzechnik (1991)
Čechite	$Pb^{[7]}(Fe^{2+},Mn^{2+})(OH)(VO_4)$	*Pnam*	7.605(3)	9.435(4)	6.099(2)	438	Mrázek and Táborský (1981), Effenberger and Pertlik (1988), Pertlik (1989)*
Pyrobelonite	$Pb^{[7]}Mn^{2+}(OH)(VO_4)$	*Pnma*	7.646(2)	6.179(1)	9.507(2)	449.15(17)	Donaldson and Barnes (1955), Barnes and Ahmed (1969), Dunn (1983), Pring et al. (1989), Rodnova (1993), Kolitsch (2001)*
synthetic	$Cd^{[7]}Cu(OH)(AsO_4)$	*Pnam*	7.418(2)	9.024(2)	5.8930(15)	394.48(15)	Effenberger (2002), this work*
synthetic	$Cd^{[7]}Co(OH)(AsO_4)$	*Pnam*	7.548(2)	8.729(2)	6.0560(10)	399.01(15)	this work
synthetic	$Cd^{[7]}Cu(OH)(VO_4)$	*Pnam* (?)	7.370(1)	5.826(1)	9.368(2)	402.24(12)	this work
synthetic	$Cd^{[7]}Co(OH)(VO_4)$	*Pnam* (?)	7.561(2)	8.873(2)	5.9990(10)	402.47(16)	this work
synthetic	$Hg^{[7]}Zn(OH)(AsO_4)$	*Pnma*	7.6826(7)	6.2459(6)	8.6691(8)	415.98(7)	Weil (2004)
synthetic	$(Pb_{0.7}Fe^{3+}_{0.3})Cu(OH)_{0.5}O_{0.4}(VO_4)$***	*Pnma*	7.525(7)	5.900(3)	9.640(5)	427.99	Permer et al. (1993)
synthetic	$Na^{[7]}Cu(OH)(MoO_4)$	*Pnma*	7.726 (2)	5.968(2)	9.495(3)	437.8(1)	Moini et al. (1986)
synthetic	$Na^{[7]}Zn(OH)(MoO_4)$	*Pnam*	7.850(1)	9.2922(8)	6.148(1)	444.4	Clearfield et al. (1977), Marsh and Schomaker (1979)*

** See text for discussion of atomic arrangement of $NaZn^{[4]}(SiO_3OH)$.

*** The substitution of Fe^{3+} for Pb in $(Pb_{0.7}Fe^{3+}_{0.3})Cu(VO_4)(OH)_{0.5}O_{0.4}$ (Permer et al. 1993) is highly doubtful. For the synthesis of this compound, NaF was used as a mineralizer, therefore Na may have replaced Pb; neither this nor the relation to descloizite or mottramite was discussed by these authors.

Table 2: Crystal data, data collection and refinement details for **1**-**5** and **8**.

Compound (no. in text)	**1**	**2**	**3**	**4**	**5**	**8** (conichalcite)
Crystal data						
Chemical formula	$CdCo(OH)(AsO_4)$	$CdCu(OH)(AsO_4)$	$SrCo(OH)(AsO_4)$	$SrZn(OH)(AsO_4)$	$SrCu(OH)(VO_4)$	$Ca(Cu_{0.92}Mg_{0.08})(OH)(AsO_4)$
Space group, Z	*Pnam*, 4	*Pnam*, 4	$P2_12_12_1$, 4	$P2_12_12_1$, 4	$P2_12_12_1$, 4	$P2_12_12_1$, 4
9a (Å)	7.548(2)	7.418(2)	7.608(2)	7.6454(12)	7.573(2)	7.4040(15)
b (Å)	8.729(2)	9.024(2)	9.239(2)	9.2632(19)	9.639(2)	9.2410(18)
c (Å)	6.0560(10)	5.8930(10)	6.0270(10)	6.0298(12)	5.8860(10)	5.8310(12)
V (Å^3)	399.01(15)	394.48(15)	423.64(16)	427.04(14)	429.66(16)	398.96(14)
Calculated density, D_x (g/cm^3)	5.448	5.588	4.742	4.805	4.377	4.247
Absorption coefficient, μ (mm^{-1})	17.617	19.006	24.165	25.706	19.311	14.255
Transmission factors, T_{min} / T_{max}	0.208 / 0.620	0.209 / 0.702	0.122 / 0.644	0.148 / 0.627	0.445 / 0.699	0.482 / 0.764
F (000)	596	604	560	568	556	489
Crystal size (mm^3)	0.03×0.04×0.13	0.02×0.03×0.12	0.02×0.02×0.15	0.02×0.02×0.12	0.02×0.02×0.05	0.02×0.03×0.06
Data collection						
Crystal-detector distance (mm)	30	30	30	30	30	30
Rotation width (°)	1	2	2	2	2	2
Total no. of frames	845	465	386	524	479	505
Collection time per frame (s)	170	160	320	145	80	160
Absorption correction	multi-scan	multi-scan	multi-scan	multi-scan	multi-scan	multi-scan
Range of Miller indices	$-10 \le h \le 10$ $-12 \le k \le 12$ $-8 \le l \le 8$	$-10 \le h \le 10$ $-12 \le k \le 12$ $-8 \le l \le 8$	$-10 \le h \le 10$ $-12 \le k \le 13$ $-8 \le l \le 8$	$-11 \le h \le 11$ $-14 \le k \le 14$ $-9 \le l \le 9$	$-10 \le h \le 10$ $-12 \le k \le 13$ $-8 \le l \le 8$	$-11 \le h \le 11$ $-14 \le k \le 14$ $-9 \le l \le 9$
Reflections collected / unique	4177 / 639	1095 [a] / 634	4674 / 1242	6036 / 1558	4844/ 1263	1739[a] / 1660
Observed reflections [$I > 2\sigma(I)$]	606	606	1194	1467	1136	1739
R_{int}	0.0246	0.0061	0.0337	0.0453	0.0321	0.0203

θ_{max} (°)	30.043	30.016	30.025	32.545	30.068	34.864
Refinement						
Extinction coefficient, k [b]	0.0077(7)	0.0062(4)	0.0043(7)	0.0013(6)	0.0049(9)	0.0073(8)
Refined parameters	50	50	78	79	79	81
Flack parameter (Flack, 1983), x or twin ratio	n/a	n/a	0.022(6)	0.446(19):0.554(19)	0.348(15):0.652(15)	0.037(15)
R-indices [$F^2 > 2\sigma(F^2)$] [c]	$R_1 = 0.0281$ $wR_2 = 0.0660$	$R_1 = 0.0153$ $wR_2 = 0.0382$	$R_1 = 0.0190$ $wR_2 = 0.0471$	$R_1 = 0.0283$ $wR_2 = 0.0645$	$R_1 = 0.0267$ $wR_2 = 0.0533$	$R_1 = 0.0183$ $wR_2 = 0.0455$
R-indices (all data) [c]	$R_1 = 0.0299$ $wR_2 = 0.0672$	$R_1 = 0.0165$ $wR_2 = 0.0386$	$R_1 = 0.0207$ $wR_2 = 0.048$	$R_1 = 0.0322$ $wR_2 = 0.0660$	$R_1 = 0.0337$ $wR_2 = 0.0573$	$R_1 = 0.0202$ $wR_2 = 0.0462$
Goodness-of-fit, S	1.149	1.204	1.066	1.069	1.092	1.087
$(\Delta/\sigma)_{max}$	0.000	0.000	0.001	0.001	0.000	0.001
$\Delta\rho_{min}$, $\Delta\rho_{max}$ (e/Å^3)	-1.833/2.041	-0.826/0.975	-0.700/0.804	-1.078/2.534	-0.774/1.006	-0.604/0.870

[a] Data collection for **2** was performed assuming orthorhombic symmetry; data collection for **8** was performed assuming triclinic symmetry but the diffractometer's processing software at that time averaged all reflections before creating the hkl-file, resulting in the comparatively "low" value for the number of collected reflections.

[b] $F_c^* = kF_c[1 + 0.001 \times F_c^2 \lambda^3/\sin(2\theta)]^{-1/4}$.

[c] $w = 1/[\sigma^2(F_o^2) + (0.0244P)^2 + 3.8563P]$ for **1**, $w = 1/[\sigma^2(F_o^2) + (0.0173P)^2 + 0.6367P]$ for **2**, and $w = 1/[\sigma^2(F_o^2) + (0.0245P)^2 + 0.4124P]$ for **3**, $w = 1/[\sigma^2(F_o^2) + (0.0257P)^2 + 1.8644P]$ for **4**, $w = 1/[\sigma^2(F_o^2) + (0.0245P)^2 + 0.4124P]$ for **5**, and $w = 1/[\sigma^2(F_o^2) + (0.0186P)^2 + 0.4070P]$ for **8**, where $P = (F_o^2 + 2F_c^2)/3$.

Table 3: Fractional atomic coordinates and equivalent isotropic displacement parameters for **1**-**5** and **8**.

Atom	*x*	*y*	*z*	U_{eq} (Å^2)
1				
Cd	0.12851(6)	0.17438(5)	0.25	0.02177(19)
Co	0.0	0.5	0.5	0.00624(19)
As	0.12919(7)	-0.17240(6)	0.25	0.00593(17)
O1	-0.1206(4)	0.2786(3)	0.5170(5)	0.0131(6)
O2	-0.0325(6)	-0.0418(6)	0.25	0.0244(10)
O3	0.3121(5)	-0.0576(5)	0.25	0.0107(7)
O4	0.1426(5)	0.4209(4)	0.25	0.0077(7)
H	0.253(4)	0.455(8)	0.25	0.013(18)
2				
Cd	0.12247(3)	0.18210(3)	0.25	0.01365(10)
Cu	0.0	0.5	0.5	0.00785(11)
As	0.13007(4)	-0.16215(3)	0.25	0.00647(10)
O1	-0.12416(19)	0.26519(17)	0.5112(3)	0.0123(3)
O2	-0.0354(3)	-0.0357(3)	0.25	0.0208(5)
O3	0.3164(3)	-0.0496(3)	0.25	0.0124(4)
O4	0.1361(3)	0.4285(2)	0.25	0.0076(4)
H	0.244(3)	0.466(4)	0.25	0.009(9)
3				
Sr	0.63634(4)	0.33216(3)	0.47652(5)	0.01038(9)
Co	0.24221(6)	0.49497(6)	0.24392(7)	0.00951(11)
As	0.61651(4)	0.68611(3)	0.51198(5)	0.00823(9)
O1	0.4407(3)	0.5719(2)	0.4927(4)	0.0116(4)
O2	0.7877(3)	0.5750(3)	0.5630(4)	0.0141(5)
O3	0.3605(3)	0.2778(3)	0.2295(4)	0.0116(4)
O4	0.3941(3)	0.2954(3)	0.7627(4)	0.0120(5)
O5	0.1048(3)	0.4339(2)	0.5032(4)	0.0099(4)
H	0.003(5)	0.479(5)	0.509(9)	0.021(16)

4				
Sr	0.63593(7)	0.33104(6)	0.47597(10)	0.01138(14)
Zn	0.23589(9)	0.49267(10)	0.23874(12)	0.01274(17)
As	0.61913(7)	0.68316(6)	0.51240(10)	0.00774(14)
O1	0.4438(5)	0.5707(4)	0.4921(8)	0.0111(8)
O2	0.7898(6)	0.5739(5)	0.5632(9)	0.0157(9)
O3	0.3585(6)	0.2740(5)	0.2288(7)	0.0112(8)
O4	0.3935(6)	0.2915(5)	0.7625(7)	0.0114(8)
O5	0.1106(5)	0.4348(4)	0.5045(7)	0.0095(7)
H	0.004(6)	0.471(10)	0.498(19)	0.06(4)
5				
Sr	0.63486(5)	0.32637(3)	0.47982(6)	0.01220(11)
Cu	0.24713(7)	0.49963(7)	0.24929(8)	0.01095(12)
V	0.61032(8)	0.66918(6)	0.50929(11)	0.00904(13)
O1	0.4286(3)	0.5527(3)	0.4957(5)	0.0116(5)
O2	0.7865(4)	0.5659(3)	0.5514(5)	0.0167(7)
O3	0.3684(5)	0.2612(3)	0.2348(5)	0.0154(6)
O4	0.3939(4)	0.2755(3)	0.7609(5)	0.0159(7)
O5	0.1104(3)	0.4388(3)	0.5020(5)	0.0117(5)
H1	0.014(7)	0.478(4)	0.501(8)	0.013(11)
8				
Ca	0.63268(5)	0.32352(4)	0.47987(8)	0.01121(10)
Cu	0.24585(4)	0.49958(4)	0.24995(5)	0.00854(8)
Mg	0.24585(4)	0.49958(4)	0.24995(5)	0.00854(8)
As	0.61737(2)	0.668890(19)	0.51430(4)	0.00748(6)
P	0.61737(2)	0.668890(19)	0.51430(4)	0.00748(6)
O1	0.43839(18)	0.55133(15)	0.4957(3)	0.0116(3)
O2	0.7894(2)	0.55751(18)	0.5816(3)	0.0156(3)
O3	0.3612(2)	0.25785(15)	0.2356(3)	0.0118(3)
O4	0.3993(2)	0.27997(17)	0.7572(3)	0.0128(3)
O5	0.11122(18)	0.43225(14)	0.5035(3)	0.0095(2)
H	0.028(6)	0.477(4)	0.493(7)	0.042(12)

Table 4: Anisotropic displacement parameters (Å^2) for **1**-**5** and **8**.

Atom	U_{11}	U_{22}	U_{33}	U_{23}	U_{13}	U_{12}
1						
Cd	0.0161(3)	0.0075(2)	0.0418(3)	0.0	0.0	0.00137(14)
Co	0.0074(3)	0.0062(3)	0.0052(3)	-0.0004(2)	0.0003(2)	0.0002(2)
As	0.0065(3)	0.0044(3)	0.0069(3)	0.0	0.0	-0.00152(16)
O1	0.0213(14)	0.0091(12)	0.0089(12)	0.0018(10)	-0.0002(11)	-0.0065(10)
O2	0.013(2)	0.016(2)	0.044(3)	0.0	0.0	0.0069(17)
O3	0.0096(17)	0.0143(18)	0.0082(16)	0.0	0.0	-0.0067(15)
O4	0.0058(15)	0.0098(17)	0.0076(15)	0.0	0.0	-0.0006(12)
O5	0.0161(3)	0.0075(2)	0.0418(3)	0.0	0.0	0.00137(14)
2						
Cd	0.01208(14)	0.00867(13)	0.02021(15)	0.0	0.0	0.00081(8)
Cu	0.00766(19)	0.01040(18)	0.00548(18)	-0.00086(11)	0.00029(14)	0.00177(11)
As	0.00666(16)	0.00659(15)	0.00615(15)	0.0	0.0	-0.00061(10)
O1	0.0175(8)	0.0109(7)	0.0086(7)	0.0026(6)	0.0007(6)	-0.0037(6)
O2	0.0113(11)	0.0176(11)	0.0335(15)	0.0	0.0	0.0067(10)
O3	0.0123(10)	0.0162(11)	0.0088(10)	0.0	0.0	-0.0094(9)
O4	0.0071(9)	0.0078(10)	0.0079(9)	0.0	0.0	0.0006(7)
O5	0.01208(14)	0.00867(13)	0.02021(15)	0.0	0.0	0.00081(8)
3						
Sr	0.01025(14)	0.00877(15)	0.01212(15)	-0.00008(11)	0.00041(11)	0.00057(11)
Co	0.0105(2)	0.0107(2)	0.0074(2)	0.00093(14)	0.00103(17)	0.00029(14)
As	0.00822(15)	0.00849(16)	0.00798(15)	0.00001(11)	0.00020(12)	-0.00070(11)
O1	0.0111(10)	0.0138(11)	0.0100(10)	-0.0004(9)	0.0005(10)	-0.0058(9)
O2	0.0120(11)	0.0122(11)	0.0182(12)	0.0003(9)	-0.0001(9)	0.0057(10)
O3	0.0154(12)	0.0110(10)	0.0084(10)	-0.0030(9)	0.0004(9)	0.0041(10)
O4	0.0167(12)	0.0105(10)	0.0089(10)	0.0028(8)	0.0011(9)	0.0028(10)
O5	0.0115(10)	0.0097(11)	0.0086(10)	0.0002(8)	0.0000(10)	-0.0003(8)
4						
Sr	0.0108(2)	0.0093(2)	0.0141(3)	0.0001(2)	0.0007(2)	0.00057(18)
Zn	0.0138(3)	0.0172(3)	0.0072(3)	0.0031(3)	0.0019(3)	-0.0009(2)
As	0.0075(2)	0.0093(3)	0.0064(3)	0.0002(2)	0.0006(2)	-0.00019(18)
O1	0.0130(18)	0.0117(19)	0.008(2)	0.0014(17)	0.0021(17)	-0.0037(14)
O2	0.0124(19)	0.016(2)	0.019(2)	-0.0005(17)	-0.0012(18)	0.0041(17)

O3	0.014(2)	0.0145(19)	0.0054(17)	-0.0002(15)	-0.0009(16)	0.0038(17)
O4	0.0157(19)	0.0125(19)	0.0060(18)	0.0032(15)	-0.0021(16)	0.0015(15)
O5	0.0078(17)	0.0121(19)	0.0086(18)	-0.0005(15)	-0.0011(17)	-0.0001(13)
5						
Sr	0.0113(2)	0.0121(2)	0.0133(2)	0.0004(2)	0.0004(2)	0.00032(17)
Cu	0.0107(3)	0.0151(3)	0.0070(3)	0.0009(2)	-0.0001(2)	-0.00255(18)
V	0.0094(4)	0.0097(4)	0.0080(4)	-0.0004(4)	0.0002(4)	-0.0003(3)
O1	0.0106(15)	0.0152(16)	0.0089(18)	-0.0003(14)	-0.0008(17)	-0.0033(12)
O2	0.0110(17)	0.017(2)	0.022(2)	-0.0007(15)	-0.0012(16)	0.0020(14)
O3	0.014(2)	0.019(2)	0.0132(19)	-0.0009(14)	-0.0007(19)	0.0031(19)
O4	0.018(3)	0.019(2)	0.0108(19)	0.0015(15)	0.0020(17)	0.0019(16)
O5	0.0094(17)	0.0160(18)	0.0098(17)	0.0021(15)	-0.0002(19)	0.0010(13)
8						
Ca	0.01115(17)	0.01036(16)	0.01211(17)	0.00019(14)	0.00018(14)	0.00051(12)
Cu	0.00811(12)	0.01172(12)	0.00578(12)	0.00124(7)	0.00012(8)	-0.00207(6)
Mg	0.00811(12)	0.01172(12)	0.00578(12)	0.00124(7)	0.00012(8)	-0.00207(6)
As	0.00733(9)	0.00836(8)	0.00675(8)	0.00001(7)	0.00012(7)	-0.00057(6)
P	0.00733(9)	0.00836(8)	0.00675(8)	0.00001(7)	0.00012(7)	-0.00057(6)
O1	0.0114(6)	0.0136(6)	0.0099(6)	-0.0009(6)	-0.0009(6)	-0.0043(4)
O2	0.0113(7)	0.0161(7)	0.0194(8)	0.0010(6)	-0.0024(6)	0.0056(6)
O3	0.0140(7)	0.0142(7)	0.0072(6)	-0.0017(5)	0.0012(5)	0.0013(6)
O4	0.0161(7)	0.0137(6)	0.0086(6)	0.0032(5)	0.0018(6)	0.0038(6)
O5	0.0074(5)	0.0127(5)	0.0084(5)	0.0001(5)	-0.0003(7)	0.0003(4)

Table 5. Selected bond distances (Å) and bond angles (°) for **1**-**5** and **8**.

	1	**2**		**3**	**4**	**5**	**8**
*M*1—O4	2.155(4)	2.226(2)	*M*1—O5	2.472(3)	2.473(4)	2.511(4)	2.3708(18)
—O2	2.244(5)	2.288(3)	—O4	2.547(3)	2.560(4)	2.558(5)	2.400(2)
—O3	2.454(4)	2.538(3)	—O3	2.575(3)	2.592(5)	2.565(3)	2.486(2)
—O1 ×2	2.524(3)	2.4755(16)	—O2	2.622(3)	2.646(4)	2.581(5)	2.525(2)
—O1 ×2	2.642(3)	2.5056(16)	—O3	2.660(3)	2.647(4)	2.611(4)	2.537(2)
			—O1	2.670(3)	2.664(4)	2.613(3)	2.551(2)
			—O4	2.698(3)	2.689(5)	2.685(3)	2.593(2)
			—O2	2.704(3)	2.701(5)	2.791(4)	2.633(2)
<*M*1[7]—O>	2.455	2.431	<*M*1[8]—O>	2.618	2.535	2.614	2.512
*M*2—O4 ×2	1.982(2)	1.8989(13)	*M*2—O5	1.963(3)	1.942(4)	1.905(4)	1.889(2)
—O3 ×2	2.135(3)	2.0556(15)	—O5	1.972(3)	1.955(4)	1.907(4)	1.892(2)
—O1 ×2	2.139(3)	2.3114(16)	—O1	2.147(3)	2.108(4)	2.063(4)	2.069(2)
			—O1	2.199(3)	2.233(5)	2.063(4)	2.077(2)
			—O4	2.201(3)	2.236(5)	2.418(4)	2.304(2)
			—O3	2.244(3)	2.320(4)	2.476(4)	2.393(2)
<*M*2—O>	2.085	2.089	<*M*2—O>	2.121	2.132	2.139	2.104
X—O2	1.670(5)	1.676(2)	*X*—O2	1.686(3)	1.680(5)	1.683(4)	1.680(2)
—O1 ×2	1.689(3)	1.6873(15)	—O3	1.693(3)	1.689(4)	1.696(4)	1.684(2)
—O3	1.706(4)	1.715(2)	—O4	1.695(3)	1.691(4)	1.697(4)	1.686(2)
			—O1	1.707(3)	1.702(4)	1.777(3)	1.7170(18)
<*X*—O>	1.688	1.684	<*X*—O>	1.695	1.691	1.713	1.692
O2—*X*—O1 ×2	110.28(13)	110.87(7)	O3—*X*—O2	112.41(17)	112.2(2)	111.0(2)	115.45(11)
O1—*X*—O1	113.28(19)	113.04(11)	O3—*X*—O4	113.31(15)	113.7(2)	111.17(16)	113.21(9)
O2—*X*—O3	101.0(2)	100.76(13)	O2—*X*—O4	104.67(16)	104.8(2)	104.74(19)	104.09(11)
O1—*X*—O3 ×2	110.68(12)	110.32(6)	O3—*X*—O1	109.38(16)	108.8(2)	111.4(2)	109.11(10)
			O2—*X*—O1	103.95(16)	104.8(2)	104.29(17)	102.23(10)
			O4—*X*—O1	112.70(15)	112.1(2)	113.73(18)	112.24(10)

<O—*X*—O>	109.37	109.36	<O—*X*—O>	109.40	109.40	109.39	109.39
O4—*M*2—O4	180.0(2)	180.00(10)	O5—*M*2—O5	174.53(13)	170.64(17)	178.38(16)	177.74(8)
O4—*M*2—O3 ×2	95.68(11)	97.46(7)	O5—*M*2—O1	97.66(13)	100.62(18)	97.96(15)	97.94(8)
O4—*M*2—O3 ×2	84.32(11)	82.54(7)	O5—*M*2—O1	87.71(12)	87.57(17)	83.68(15)	84.28(8)
O3—*M*2—O3	180.0	180.0	O5—*M*2—O1	85.27(12)	83.13(16)	83.64(15)	84.15(8)
O4—*M*2—O1 ×2	87.32(13)	85.55(7)	O5—*M*2—O1	89.34(12)	88.67(17)	94.72(15)	93.63(8)
O4—*M*2—O4 ×2	92.68(13)	94.45(7)	O1—*M*2—O1	176.96(12)	176.18(18)	178.31(15)	177.81(9)
O3—*M*2—O1 ×2	92.05(14)	92.53(8)	O5—*M*2—O4	91.29(12)	90.25(17)	90.78(14)	91.76(8)
O3—*M*2—O1 ×2	87.95(14)	87.47(8)	O5—*M*2—O4	87.78(12)	88.63(17)	89.58(14)	88.88(8)
O1—*M*2—O1	180.0	180.0	O1—*M*2—O4	89.08(12)	89.00(16)	87.40(14)	84.64(8)
			O1—*M*2—O4	90.24(12)	90.33(17)	92.99(14)	95.97(8)
			O5—*M*2—O3	89.24(12)	88.77(17)	86.75(14)	84.74(7)
			O5—*M*2—O3	91.93(12)	92.32(17)	93.00(14)	94.85(7)
			O1—*M*2—O3	92.29(12)	90.72(15)	90.40(14)	89.89(7)
			O1—*M*2—O3	88.56(12)	90.12(16)	89.29(14)	89.66(7)
			O4—*M*2—O3	175.93(14)	177.40(17)	175.56(17)	173.05(8)

Hydrogen bonds

Compound	Donor	H	Acceptor	D–H	H···A	∠D–H···A	D···A
1	O4	H	O2	0.88(2)	1.79(2)	175(8)	2.670(6)
2	O4	H	O2	0.88(2)	1.75(2)	178(4)	2.622(3)
3	O5	H	O2	0.88(3)	1.89(3)	172(5)	2.766(4)
4	O5	H	O2	0.88(3)	1.93(4)	164(11)	2.793(6)
5	O5	H	O2	0.88(3)	1.88(3)	172(6)	2.756(5)
8	O5	H	O2	0.75(4)	1.98(4)	157(4)	2.688(2)

Table 6. Bond valences v_{ij} (valence units) for **1**-**5** and **8**. The calculation is based on the parameters given by Brese and O'Keeffe (1991), for the hydrogen bonds according to Ferraris and Ivaldi (1988).

	*M*1	*M*2	*X*	Σv_{ij}*	H	Σv_{ij}**
1						
O1	0.19×2 + 0.14×2	0.29×2	1.23×2	1.85	—	1.85
O2	0.40	—	1.30	1.73	0.25	1.98
O3	0.23	0.30×2	1.18	2.01	—	2.01
O4	0.51	0.46×2	—	1.43	0.75	2.18
Σv_{ij}	1.80	2.10	4.94		1.00	
2						
O1	0.21×2 + 0.20×2	0.18×2	1.24×2	1.83	—	1.83
O2	0.35	—	1.28	1.63	0.27	2.00
O3	0.18	0.36×2	1.15	2.05	—	2.05
O4	0.42	0.55×2	—	1.52	0.73	2.25
Σv_{ij}	1.77	2.18	4.91		1.00	
3						
O1	0.22	0.29 + 0.25	1.18	1.94	—	1.94
O2	0.26 + 0.20	—	1.24	1.70	0.18	1.88
O3	0.29 + 0.23	0.22	1.22	1.96	—	1.96
O4	0.31 + 0.21	0.25	1.21	1.98	—	1.98
O5	0.38	0.48 + 0.47	—	1.33	0.82	2.15
Σv_{ij}	2.10	1.96	4.85		1.00	
4						
O1	0.23	0.24 + 0.33	1.14	1.94	—	1.94
O2	0.24 + 0.21	—	1.27	1.72	0.17	1.89
O3	0.28 + 0.24	0.19	1.23	1.94	—	1.94
O4	0.30 + 0.21	0.24	1.23	1.98	—	1.98
O5	0.38	0.53 + 0.51	—	1.42	0.83	2.25
Σv_{ij}	2.09	2.04	4.92		1.00	
5						
O1	0.27	0.25 + 0.35	1.07	1.94	—	1.94
O2	0.29 + 0.16	—	1.38	1.83	0.18	2.01

O3	0.30 + 0.27	0.12	1.34	2.03	—	2.03
O4	0.30 + 0.22	0.14	1.33	1.99	—	1.99
O5	0.36	0.54 + 0.54	—	1.44	0.82	2.26
Σv_{ij}	2.17	2.04	5.12		1.00	
8						
O1	0.21	0.36 +0.34	1.14	2.05	—	2.05
O2	0.22 + 0.17	—	1.27	1.66	0.23	1.89
O3	0.26 + 0.21	0.14	1.25	1.86	—	1.86
O4	0.31 + 0.18	0.18	1.24	1.91	—	1.91
O5	0.36	0.57 + 0.56	—	1.49	0.77	2.26
Σv_{ij}	1.92	2.14			1.00	

* Neglecting the contribution from the hydrogen bonds.
** Including the contribution from the hydrogen bonds.

Table 7. Transformation and translation matrices of the unit cells and atomic coordinates for the members of the adelite and descloizite groups reported in the original work to the reference model that corresponds to the set of coordinates given by Effenberger et al. (2000) for adelite, $CaMg(OH)(AsO_4)$. Descloizite-group members were, prior to the transformation from the table, transformed to the lower-symmetry space group $P2_12_12_1$ using the program TRANSTRU (Tasci et al. 2012) hosted in the Bilbao Crystallographic Server (http://www.cryst.ehu.es).

Compound	Transformation matrix	Translation matrix	Renumbering scheme for the O sites (old → new)	Reference
Čechite	100/010/00-1	0 0 ¼	4→1, 3→2, 2→3, 1→4,	Pertlik (1989)*
Descloizite	100/00-1/010	¼ ¼ ½	4→1, 3→2, 2→3, 1→4,	Keller & Hess (1988)
Pyrobelonite	-100/001/010	¼ ¾ 0	1→1, 2→2, 3→3, 4→4,	Kolitsch (2001)
Tangeite	100/0-10/00-1	0 0 ½	1→1, 2→2, 3→3, 4→4,	Basso et al. (1989)
$SrCu(VO_4)(OH)$	100/010/001	0 0 0	1→1, 2→2, 3→3, 4→4,	this work
Mottramite	100/00-1/010	¼ ¼ ½	4→1, 5→2, 3→3, 2→4, 1→5	Cooper & Hawthorne (1995)
Arsendescloizite	-100/0-10/001	0 -½ ½	1→1, 2→2, 4→3, 3→4,	Keller et al. (2003)
Conichalcite	100/010/001	0 0 0	1→1, 2→2, 3→3, 4→4,	this work
Vuagnatite	100/010/001	0 0 0	1→1, 2→2, 3→3, 4→4,	McNear et al. (1976)
Mozartite	001/100/010	0 ½ 0	1→1, 2→2, 4→3, 3→4,	Nyfeler et al. (1997)
$CdCu(AsO_4)(OH)$	100/0-10/001	¼ 0 ¾	3→1, 2→2, 5→3, 1→4,	this work
$SrCo(AsO_4)(OH)$	001/100/010	0 0 0	1→1, 2→2, 3→3, 4→4,	this work
$SrZn(AsO_4)(OH)$	001/100/010	0 0 0	1→1, 2→2, 3→3, 4→4,	this work
$NaCu(MoO_4)(OH)$	100/001/0-10	¼ ¾ ½	3→1, 4→2, 1→3, 2→4,	Moini et al. (1976)
Hermannroseite	100/010/001	0 0 0	1→1, 2→2, 3→3, 4→4,	Schlüter et al. (2011)
Adelite	100/010/001	0 0 0	1→1, 2→2, 3→3, 4→4,	Effenberger et al. (2002)
Nickelaustinite	-100/0-10/001	0 0 -½	1→1, 2→2, 3→3, 4→4,	Cesbron et al. (1987)
Gottlobite	-100/0-10/001	0 0 ½	2→1, 5→2, 4→3, 3→4,	Witzke et al. (2000)
Austinite	100/010/001	0 0 0	1→1, 2→2, 3→3, 4→4,	Clark et al. (1997)
Cobaltaustinite	100/010/001	0 0 0	1→1, 2→2, 3→3, 4→4,	Yang et al. (2007)
$CdCo(AsO_4)(OH)$	100/0-10/001	¼ 0 ¾	3→1, 2→2, 5→3, 1→4,	this work
$NaZn(MoO_4)(OH)$	100/010/001	0 0 ¼	5→1, 3→2, 1→3, 2→4,	Marsh & Schomaker
Duftite	100/0-10/001	0 0 ½	4→1, 5→2, 3→3, 2→4,	Kharisun et al. (1998)

Table 8. The degree of lattice distortion (S) and the structure similarity (Δ) of the adelite- and descloizite-group members in comparison with the crystal structure of descloizite (Hawthorne and Faggiani 1979) transformed to space group $P2_12_12_1$, with matching coordinates to those of adelite (Effenberger et al. 2002). For more details see Supplementary Material.

Mineral name, formula	Legend	S	$d_{max.}$ (Å)	$d_{av.}$ (Å)	Δ	References
Čechite, $PbFe(VO_4)(OH)$	CECH	0.0024	0.0638	0.0351	0.012	Pertlik (1989)
Pyrobelonite, $PbMn(VO_4)(OH)$	PYBEL	0.0076	0.1292	0.0323	0.021	Kolitsch (2001)
Tangeite, $CaCu(VO_4)(OH)$	TANG	0.0150	0.4857	0.2007	0.038	Basso et al. (1989)
synthetic, $SrCu(VO_4)(OH)$	SrCuV	0.0127	0.3692	0.1807	0.043	this work
Mottramite, $PbCu(VO_4)(OH)$	MOTR	0.0048	0.1570	0.0816	0.046	Cooper & Hawthorne (1995)
Arsendescloizite, $PbZn(AsO_4)(OH)$	AsDES	0.0032	0.3195	0.1450	0.047	Keller et al. (2003)
Conichalcite, $CaCu(AsO_4)(OH)$	CONC	0.0170	0.5936	0.2161	0.047	this work
Vuagnatite, $CaAl(SiO_4)(OH)$	VUAG	0.0500	0.4556	0.1694	0.049	McNear et al. (1976)
Mozartite, $CaMn(SiO_3OH)$	MOZ	0.0341	0.4662	0.1582	0.051	Nyfeler et al. (1997)
synthetic, $CdCu(AsO_4)(OH)$	CdCuAs	0.0193	0.4868	0.1822	0.053	this work
synthetic, $SrCo(AsO_4)(OH)$	SrCoAs	0.0067	0.3977	0.1439	0.059	this work
synthetic, $SrZn(AsO_4)(OH)$	SrZnAs	0.0062	0.4007	0.1612	0.069	this work
synthetic, $NaCu(MoO_4)(OH)$	NaCuMo	0.0081	0.3639	0.1861	0.072	Moini et al. (1986)
Hermannroseite, $CaCu(PO_4,AsO_4)(OH)$	HERO	0.0237	0.6721	0.3242	0.073	Schlüter et al. (2011)
Adelite, $CaMg(AsO_4)(OH)$	ADEL	0.0197	0.5694	0.1960	0.078	Effenberger et al. (2002)
Nickelaustinite, $CaNi(AsO_4)(OH)$	NiAUS	0.0203	0.5458	0.1904	0.078	Cesbron et al. (1987)
Gottlobite, $CaMg(VO_4)(OH)$	GOTL	0.0172	0.5234	0.1863	0.081	Witzke et al. (2000)
Austinite, $CaZn(AsO_4)(OH)$	AUS	0.0161	0.5759	0.2126	0.083	Cesbron et al. (1987)

Cobaltaustinite, $CaCo(AsO_4)(OH)$	CoAUS	0.0185	0.5745	0.1958	0.084	Yang et al. (2007)
synthetic, $CdCo(AsO_4)(OH)$	CdCoAs	0.0273	0.4336	0.1403	0.090	this work
synthetic, $NaZn(MoO_4)(OH)$	NaZnMo	0.0126	0.3226	0.1416	0.091	Marsh and Schomaker (1979)
Duftite, $PbCu(AsO_4)(OH)$	DUFT	0.0110	0.2426	0.1494	0.111	Kharisun et al. (1998)

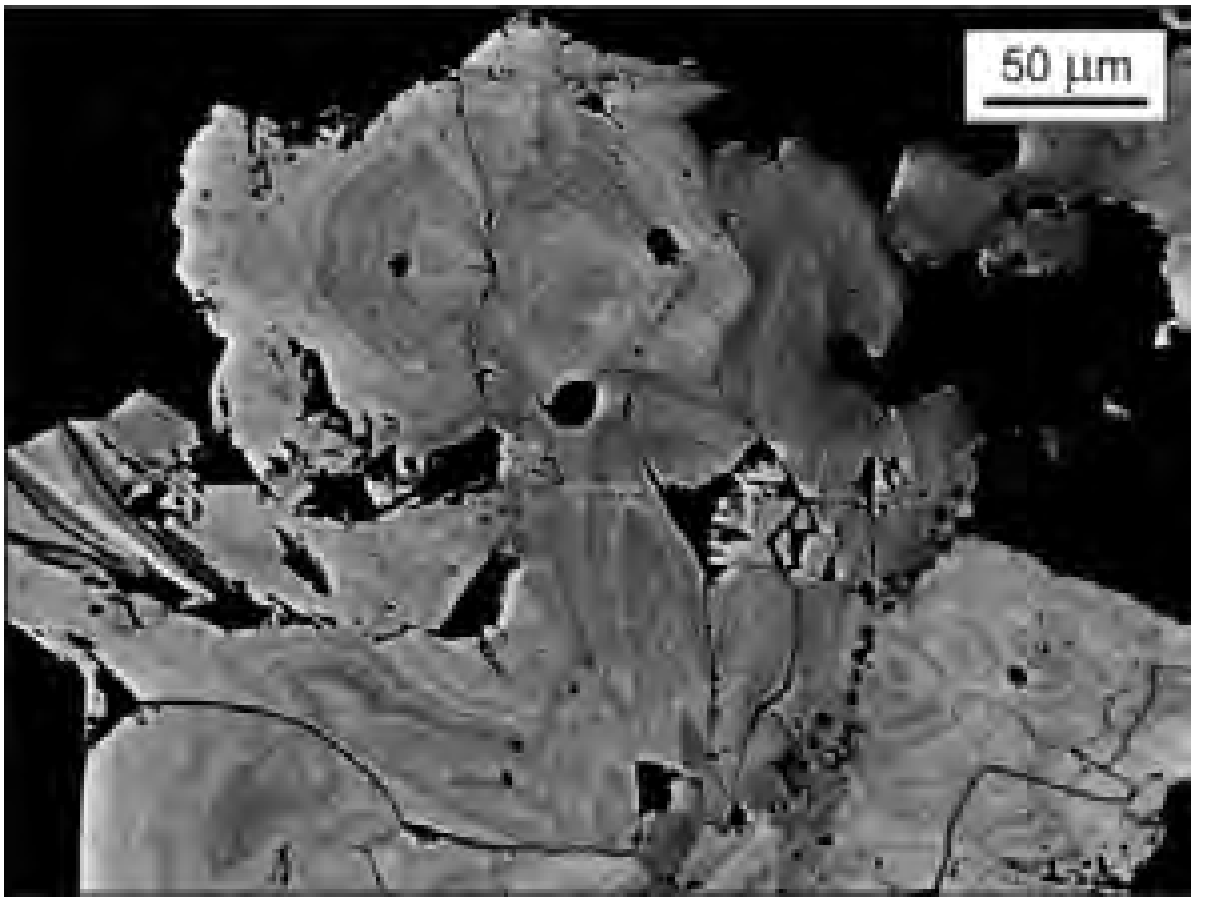
50 µm

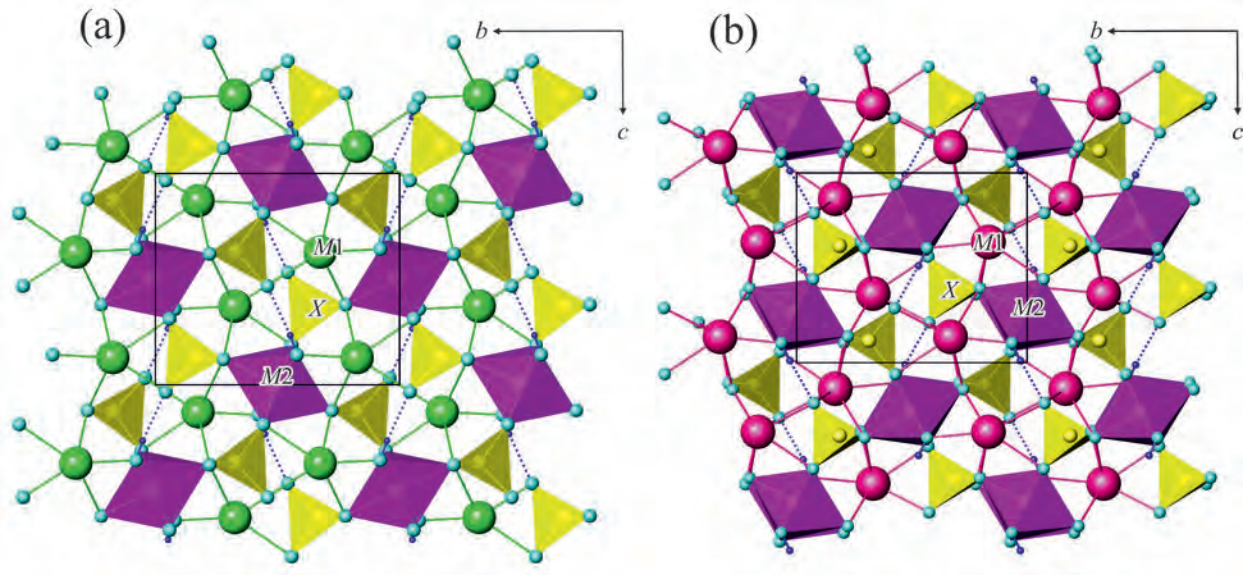
(a)
b
c
M1
X
M2
(b)
b
c
M1
X
M2

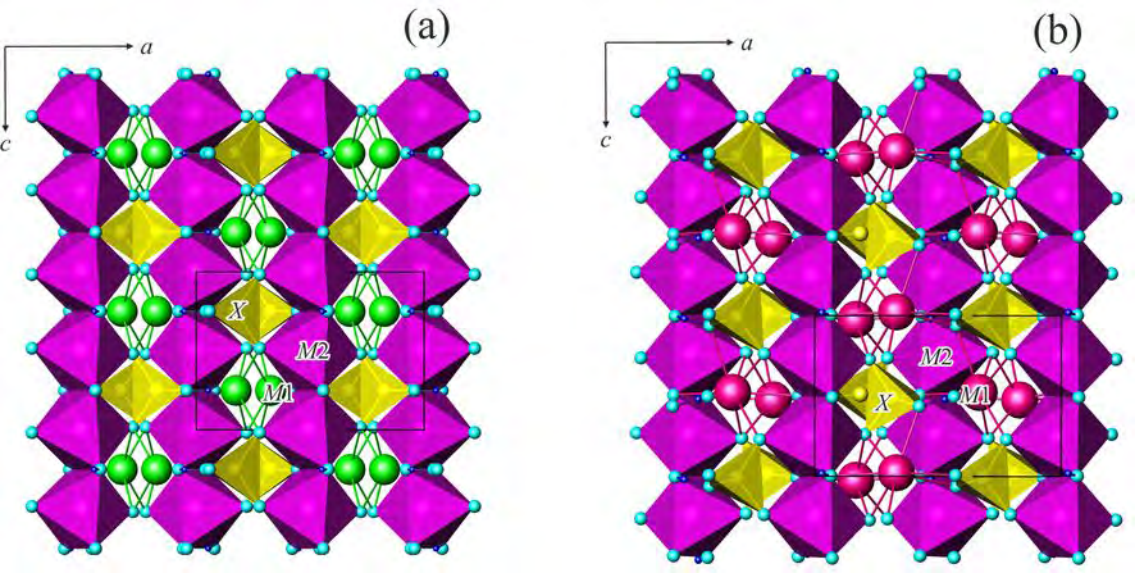
(a)
a
c
X
M2
M1
(b)
a
c
M2
X
M1

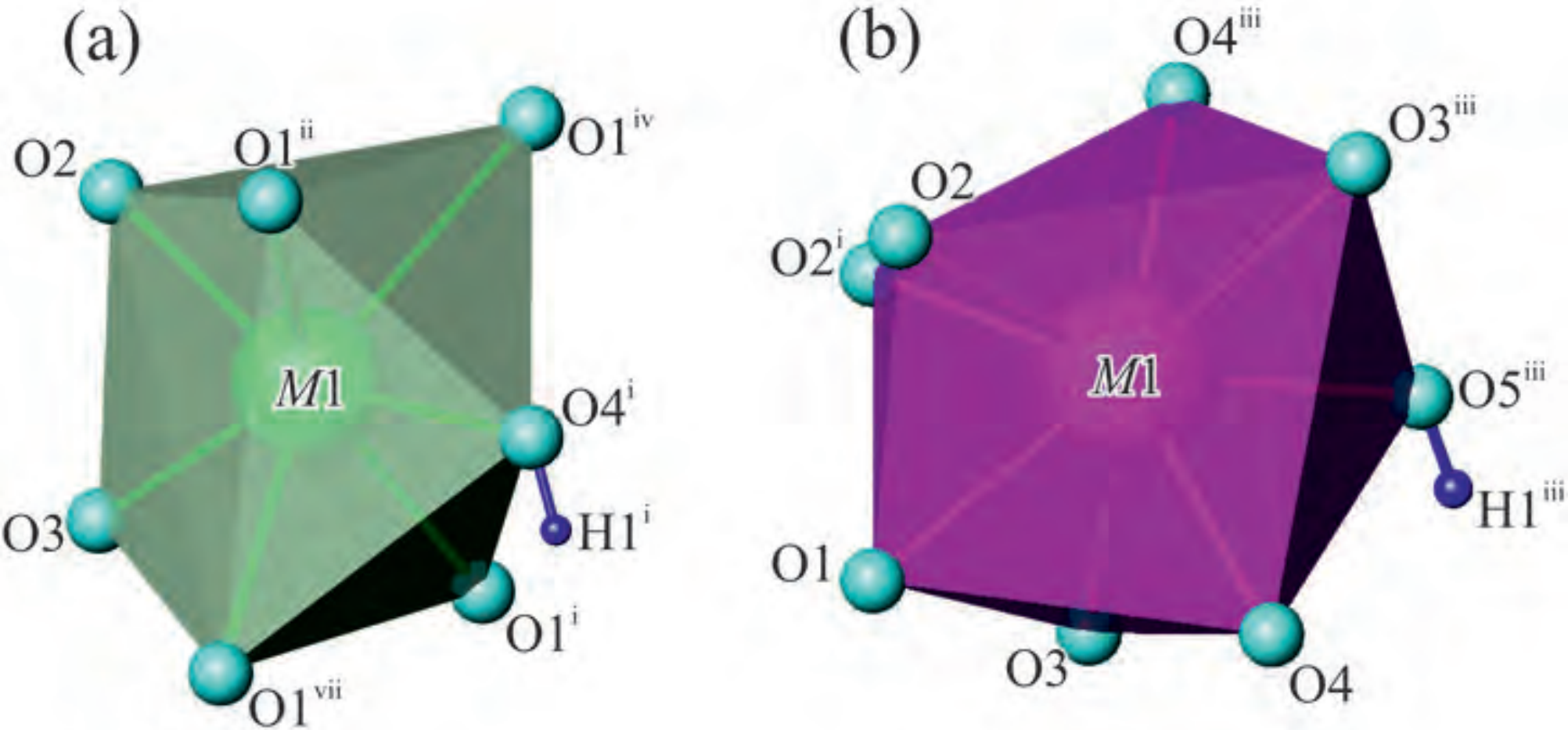
(a)
O2
O1ii
O1iv
M1
O4i
O3
H1i
O1i
O1vii
(b)
O4iii
O3iii
O2
O2i
M1
O5iii
H1iii
O1
O3
O4

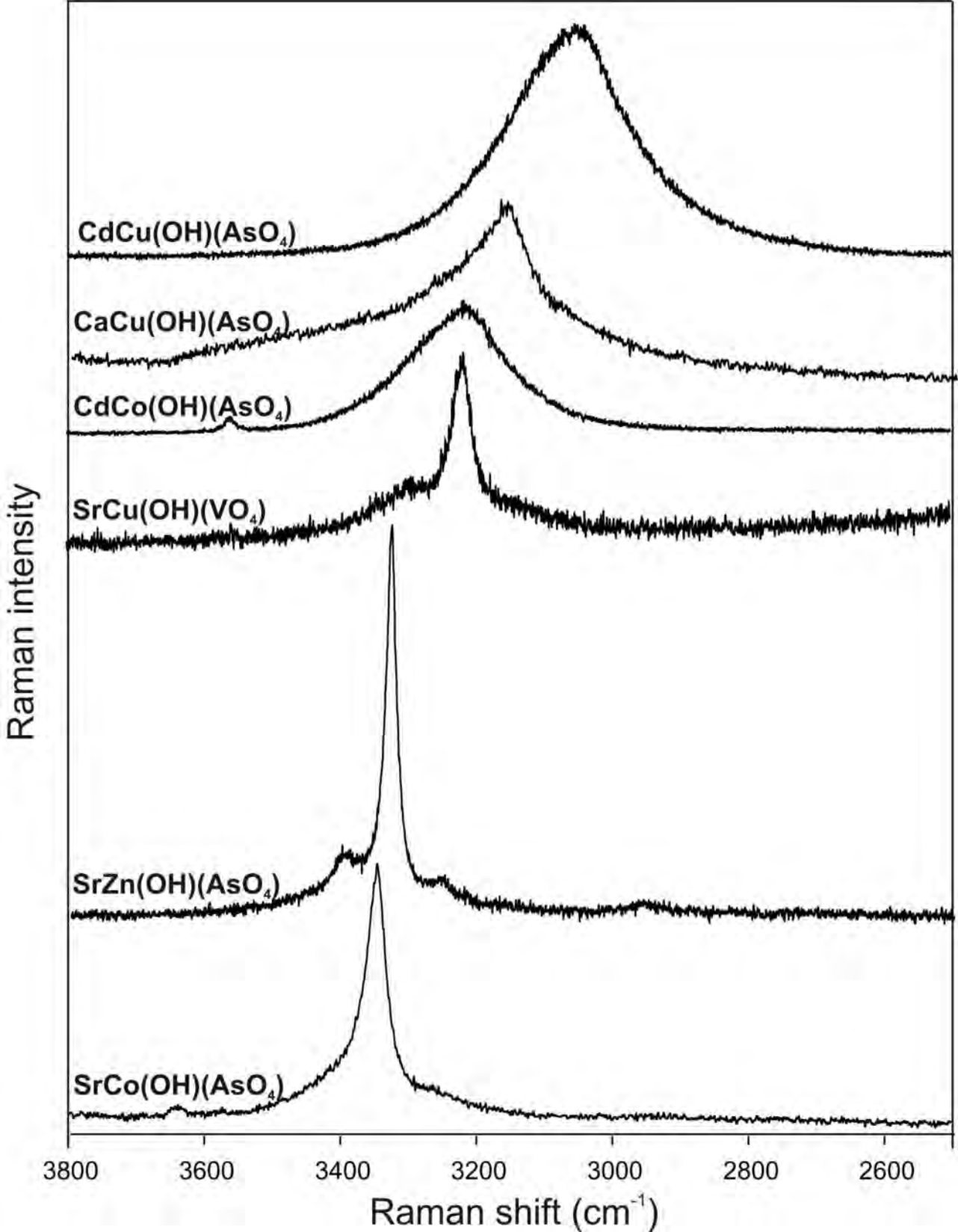
CdCu(OH)(AsO4)
CaCu(OH)(AsO4)
CdCo(OH)(AsO4)
SrCu(OH)(VO4)
SrZn(OH)(AsO4)
SrCo(OH)(AsO4)
Raman intensity
3800
3600
3400
3200
3000
2800
2600
Raman shift (cm-1)

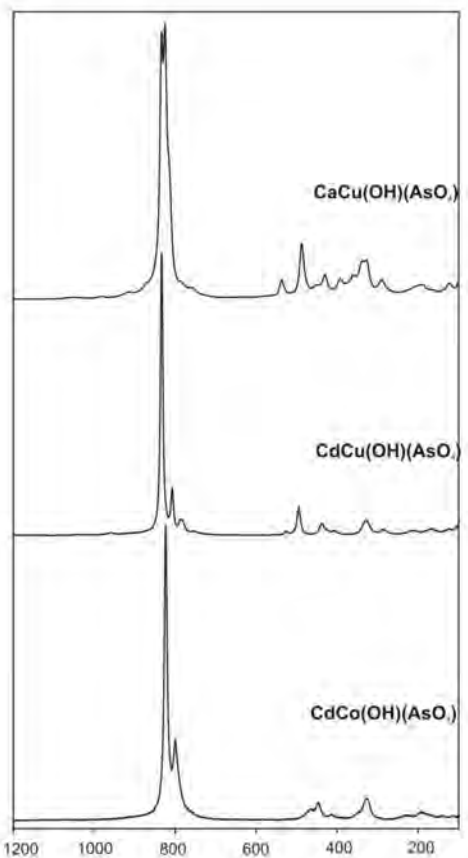
CaCu(OH)(AsO4)
CdCu(OH)(AsO4)
CdCo(OH)(AsO4)
1200
1000
800
600
400
200

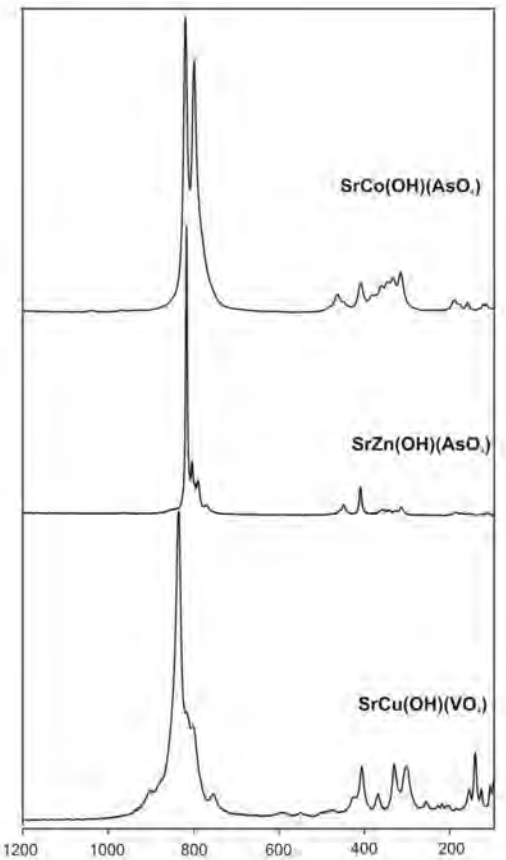
SrCo(OH)(AsO4)
SrZn(OH)(AsO4)
SrCu(OH)(VO4)
1200
1000
800
600
400
200

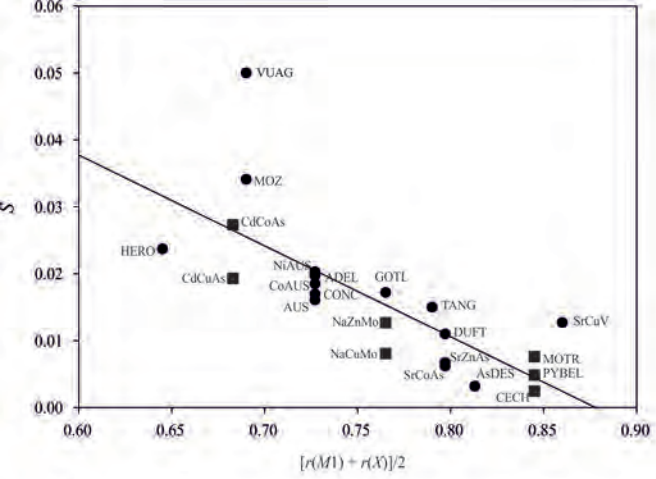
S
[r(M1) + r(X)]/2
VUAG
MOZ
CdCoAs
HERO
CdCuAs
NiAUS
ADEL
CoAUS
CONC
AUS
GOTL
TANG
NaZnMo
DUFT
NaCuMo
SrZnAs
SrCoAs
AsDES
MOTR
PYBEL
CECH
SrCuV

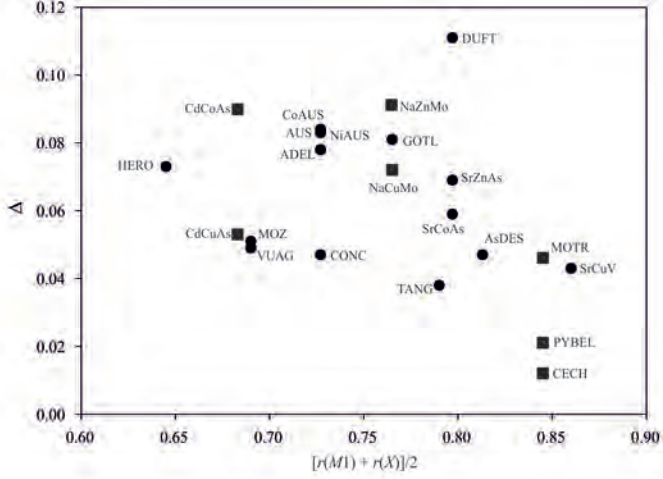
Δ
[r(M1) + r(X)]/2
DUFT
CdCoAs
NaZnMo
CoAUS
AUS
NiAUS
GOTL
ADEL
HERO
NaCuMo
SrZnAs
SrCoAs
CdCuAs
MOZ
VUAG
CONC
AsDES
MOTR
SrCuV
TANG
PYBEL
CECH

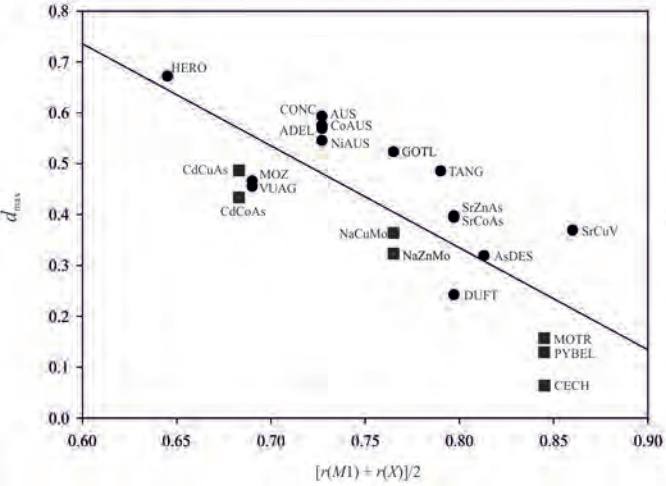
d_{max}
[r(M1) + r(X)]/2
HERO
CONC
AUS
ADEL
CoAUS
NiAUS
GOTL
CdCuAs
MOZ
TANG
VUAG
CdCoAs
SrZnAs
SrCoAs
NaCuMo
SrCuV
NaZnMo
AsDES
DUFT
MOTR
PYBEL
CECH

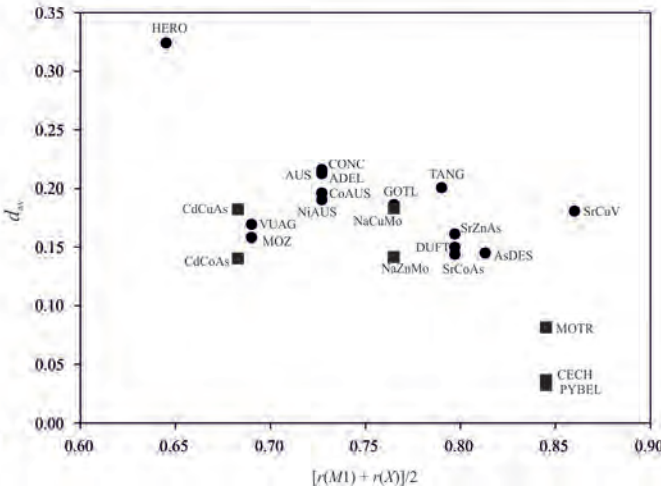
d_{av}
[r(M1) + r(X)]/2
HERO
AUS
CONC
ADEL
TANG
CoAUS
GOTL
CdCuAs
NiAUS
SrCuV
NaCuMo
VUAG
SrZnAs
MOZ
DUFT
AsDES
CdCoAs
NaZnMo
SrCoAs
MOTR
CECH
PYBEL

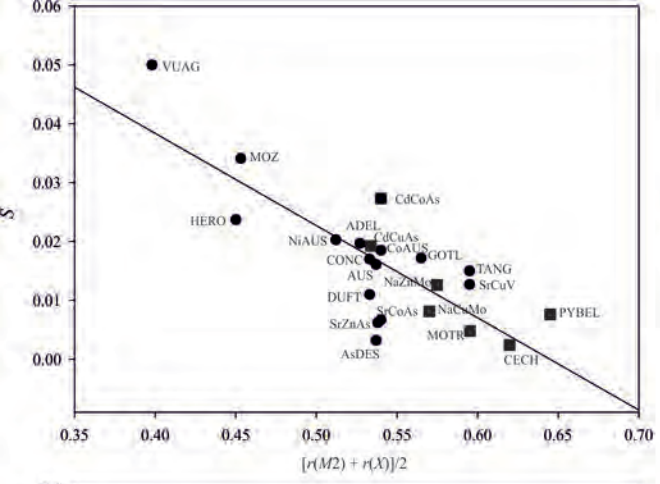
S
[r(M2) + r(X)]/2
VUAG
MOZ
HERO
CdCoAs
ADEL
NiAUS
CdCuAs
CoAUS
CONC
GOTL
AUS
TANG
NaZnMo
SrCuV
DUFT
SrCoAs
NaCuMo
PYBEL
SrZnAs
MOTR
AsDES
CECH

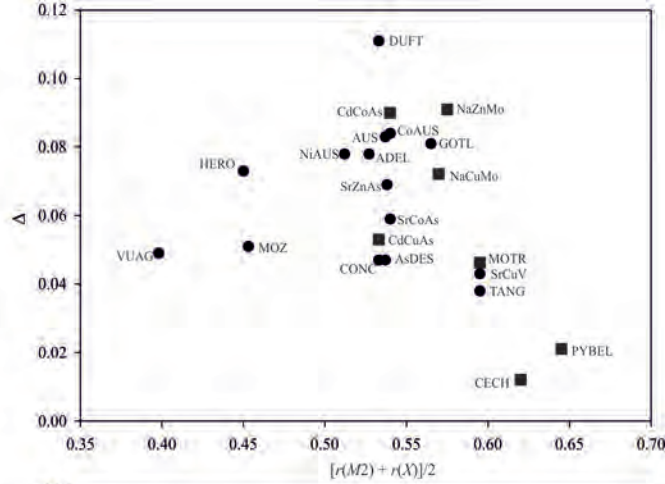
Δ
[r(M2) + r(X)]/2
DUFT
CdCoAs
NaZnMo
AUS
CoAUS
GOTL
NiAUS
ADEL
HERO
NaCuMo
SrZnAs
SrCoAs
CdCuAs
VUAG
MOZ
CONC
AsDES
MOTR
SrCuV
TANG
PYBEL
CECH

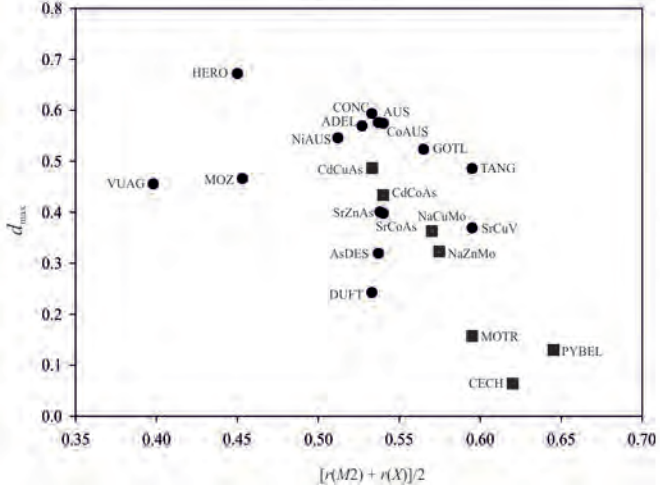
d_{max}
[r(M2) + r(X)]/2
HERO
CONC
AUS
ADEL
CoAUS
NiAUS
GOTL
CdCuAs
TANG
VUAG
MOZ
CdCoAs
SrZnAs
NaCuMo
SrCoAs
SrCuV
AsDES
NaZnMo
DUFT
MOTR
PYBEL
CECH

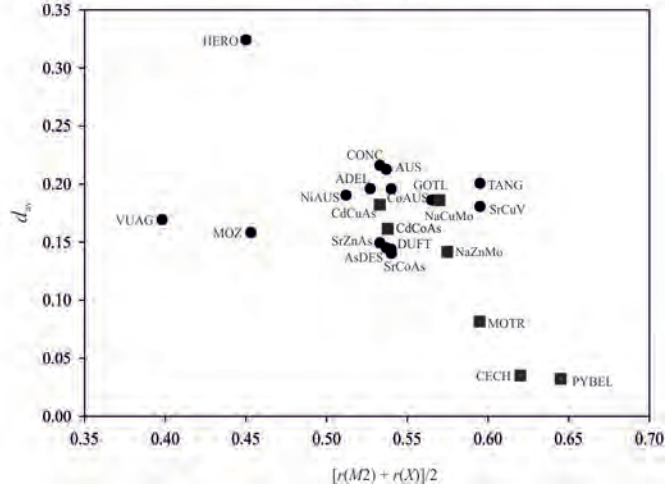
d_{av}
[r(M2) + r(X)]/2
HERO
CONC
AUS
ADEL
GOTL
TANG
NiAUS
CoAUS
CdCuAs
NaCuMo
SrCuV
VUAG
MOZ
CdCoAs
SrZnAs
DUFT
NaZnMo
AsDES
SrCoAs
MOTR
CECH
PYBEL

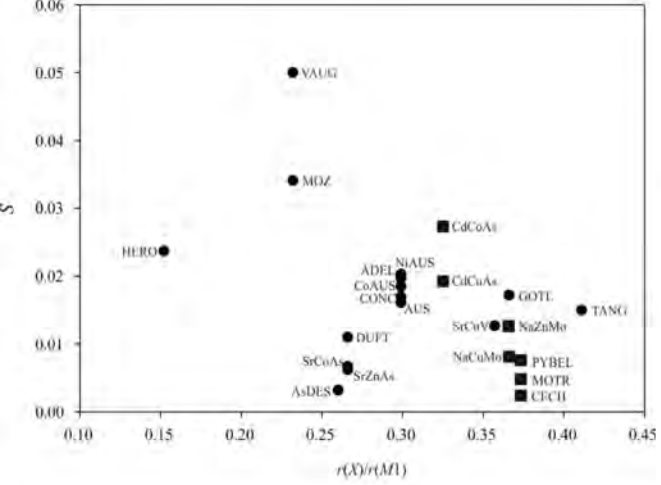
S
r(X)/r(M1)
VAUG
MOZ
HERO
CdCoAs
NiAUS
ADEL
CoAUS
CONC
AUS
CdCuAs
GOTL
TANG
SrCuV
NaZnMo
DUFT
SrCoAs
SrZnAs
NaCuMo
PYBEL
MOTR
AsDES
CECH

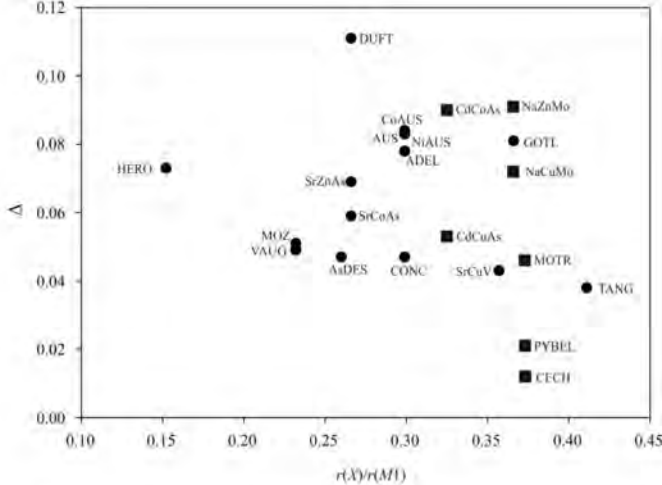
Δ
r(X)/r(M1)
DUFT
CdCoAs
NaZnMo
CoAUS
AUS
NiAUS
GOTL
ADEL
HERO
NaCuMo
SrZnAs
SrCoAs
MOZ
VAUG
CdCuAs
AsDES
CONC
SrCuV
MOTR
TANG
PYBEL
CECH

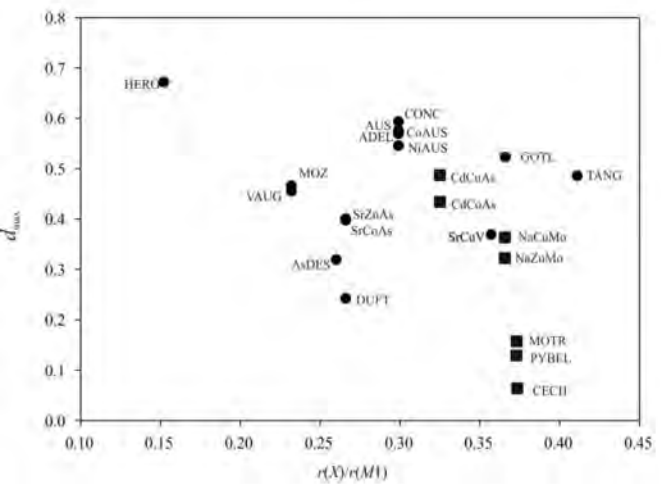
d_{max}
r(X)/r(M1)
HERO
CONC
AUS
ADEL
CoAUS
NiAUS
GOTL
MOZ
CdCuAs
TANG
VAUG
CdCuAs
SrZnAs
SrCoAs
SrCuV
NaCuMo
AsDES
NaZnMo
DUFT
MOTR
PYBEL
CECH

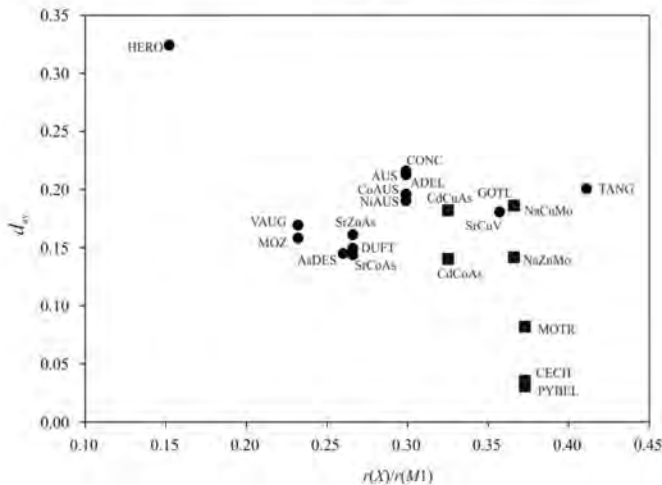
d_{av}
r(X)/r(M1)
HERO
CONC
AUS
ADEL
CoAUS
NiAUS
CdCuAs
GOTL
TANG
NaCuMo
VAUG
SrZnAs
SrCuV
MOZ
DUFT
AsDES
SrCoAs
NaZnMo
CdCoAs
MOTR
CECH
PYBEL

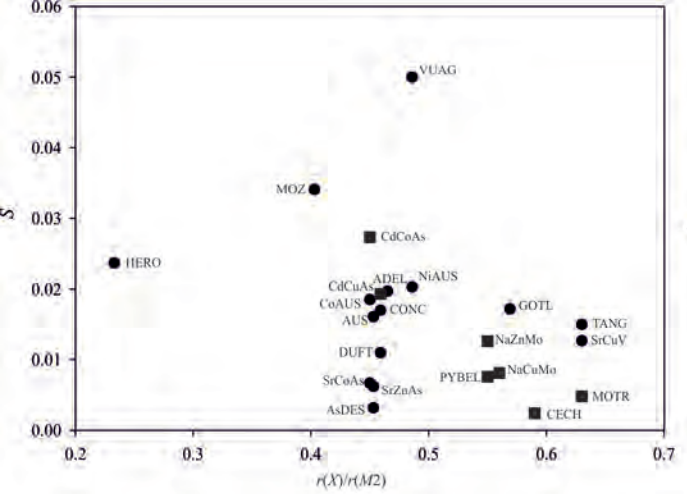
S
r(X)/r(M2)
VUAG
MOZ
HERO
CdCoAs
CdCuAs
ADEL
NiAUS
CoAUS
CONC
AUS
GOTL
TANG
NaZnMo
SrCuV
DUFT
PYBEL
NaCuMo
SrCoAs
SrZnAs
MOTR
AsDES
CECH

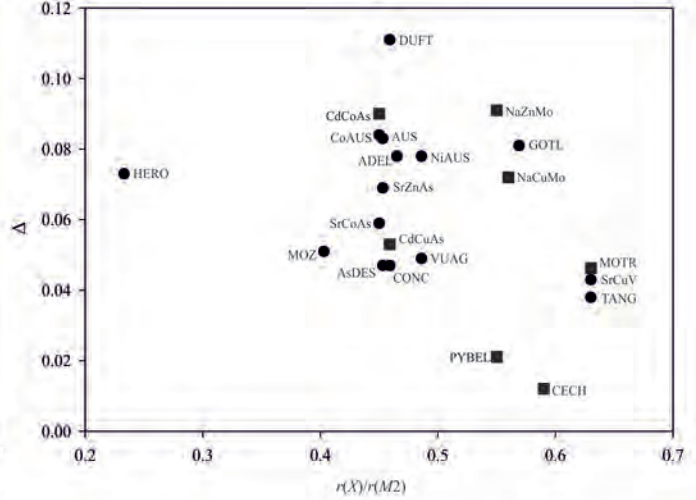
Δ
r(X)/r(M2)
DUFT
CdCoAs
NaZnMo
CoAUS
AUS
GOTL
ADEL
NiAUS
HERO
NaCuMo
SrZnAs
SrCoAs
CdCuAs
MOZ
VUAG
MOTR
AsDES
CONC
SrCuV
TANG
PYBEL
CECH

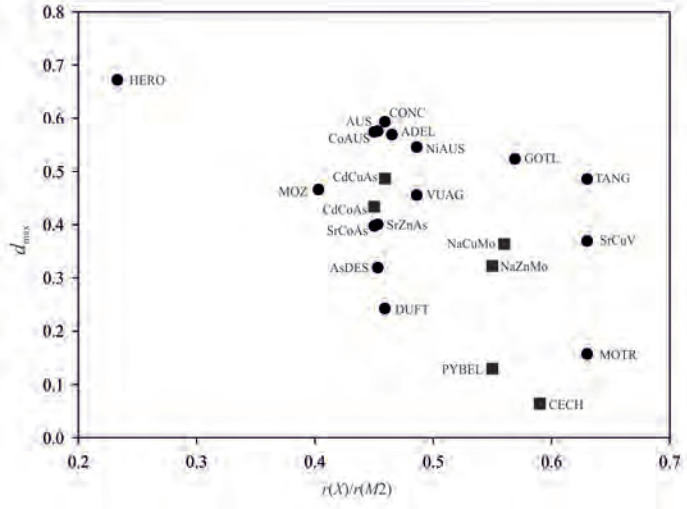
d_{max}
r(X)/r(M2)
HERO
AUS
CONC
CoAUS
ADEL
NiAUS
GOTL
TANG
MOZ
CdCuAs
VUAG
CdCoAs
SrCoAs
SrZnAs
NaCuMo
SrCuV
AsDES
NaZnMo
DUFT
MOTR
PYBEL
CECH

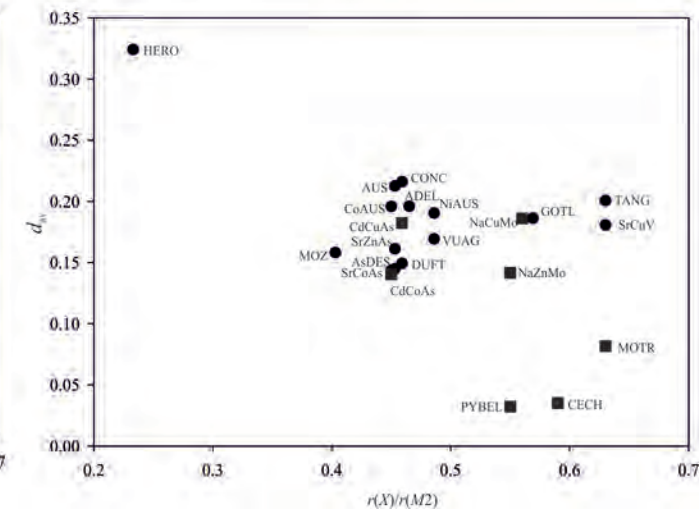
d_{av}
r(X)/r(M2)
HERO
AUS
CONC
ADEL
CoAUS
NiAUS
TANG
CdCuAs
NaCuMo
GOTL
SrCuV
SrZnAs
VUAG
MOZ
AsDES
DUFT
SrCoAs
NaZnMo
CdCoAs
MOTR
PYBEL
CECH